1 **Marine anoxia initiates giant sulfur-bacteria mat proliferation and associated changes in**

2 **benthic nitrogen, sulfur, and iron cycling in the Santa Barbara Basin, California**

3 **Borderland**

4 David J. Yousavich[1*], De'Marcus Robinson[2], Xuefeng Peng[3], Sebastian J. E. Krause[1,4], Frank

5 Wenzhöfer[5,6,7], Felix Janssen[5,6], Na Liu[8], Jonathan Tarn[8], Frank Kinnaman[8], David L. Valentine[8],

6 Tina Treude[1,2*]

8 [1]Department of Earth, Planetary, and Space Sciences, University of California Los Angeles, 595 Charles E.

9 Young Drive East, Los Angeles, CA 90095, USA

10 [2]Department of Atmospheric and Oceanic Sciences, University of California Los Angeles, Math Science

11 Building, 520 Portola Plaza, Los Angeles, CA 90095, USA

12 [3]School of Earth, Ocean, and Environment, University of South Carolina, 701 Sumter Street, EWS 617,

13 Columbia, SC 29208, USA

14 [4]Earth Research Institute, 6832 Ellison Hall, University of California Santa Barbara, Ca 93106-3060

15 [5]HGF-MPG Joint Research Group for Deep-Sea Ecology and Technology, Alfred-Wegener-Institute,

16 Helmholtz-Center for Polar and Marine Research, Am Handelshafen 12, 27570 Bremerhaven, Germany

17 [6] HGF-MPG Joint Research Group for Deep-Sea Ecology and Technology, Max Planck Institute for Marine

18 Microbiology, Celsiusstrasse 1, 28359 Bremen, Germany

19 [7]Department of Biology, DIAS, Nordcee and HADAL Centres, University of Southern Denmark, 5230 Odense

20 M, Denmark

21 [8]Department of Earth Science and Marine Science Institute, University of California, Santa Barbara, CA

22 93106, USA

24 **Correspondence:** David Yousavich (yousavdj@ucla.edu), Tina Treude (ttreude@g.ucla.edu)

Abstract

The Santa Barbara Basin naturally experiences transient deoxygenation due to its unique geological setting in the Southern California Borderland and seasonal changes in ocean currents. Long-term measurements of the basin showed that anoxic events and subsequent nitrate exhaustion in the bottom waters have been occurring more frequently and lasting longer over the past decade. One characteristic of the Santa Barbara Basin is the seasonal development of extensive mats of benthic nitrate-reducing sulfur-oxidizing bacteria, which are found at the sediment-water interface when the basin's bottom waters reach anoxia but still provide some nitrate. To assess the mat's impact on the benthic and pelagic redox environment, we collected biogeochemical sediment and benthic flux data in November 2019, after anoxia developed in the deepest waters of the basin and dissolved nitrate was depleted (down to 9.9 µM). We found that the development of mats was associated with a shift from denitrification to dissimilatory nitrate reduction to ammonium. The zone of sulfate reduction appeared near the sediment-water interface in sediment hosting these ephemeral white mats. We found that an exhaustion of iron oxides in the surface sediment was an additional prerequisite for mat proliferation. Our research further suggests that cycles of deoxygenation and reoxygenation of the benthic environment result in extremely high benthic fluxes of dissolved iron from the basin's sediment. This work expands our understanding of nitrate-reducing sulfur-oxidizing mats and their role in sustaining and potentially expanding marine anoxia.

Introduction

Naturally occurring low-oxygen waters in the ocean are commonly observed below the ocean's mixed layer where respiration consumes oxygen faster than it is produced or ventilated. When low oxygen conditions occur along the western continental shelf in regions susceptible to upwelling events and/or undergoing eutrophication, organic matter remineralization can frequently drive oxygen concentrations to hypoxic ($O_2 < 63$ μM) (Middelburg and Levin, 2009) and/or anoxic levels ($O_2 < 3$ μM) (Fossing et al., 1995; Canfield et al., 2010). These areas are usually referred to as Oxygen Minimum Zones (OMZs). In the water column of OMZs, nitrogen reduction becomes an important mechanism for organic matter remineralization (Ward et al., 2009). OMZs within coastal basins that experience seasonal changes in upwelling can experience anoxic and nitrate reducing conditions that extend to the benthic environment, especially when high productivity and associated organic matter export coincide with seasonal patterns of physical mixing. This fundamental change in the redox conditions at the sediment-water interface encourages elevated rates of anaerobic microbial processes and can promote organic matter preservation in the sediments (Middelburg and Levin, 2009; Treude, 2011), though a recent study suggests a thin reactive surface layer can provide high rates of organic matter degradation in anoxic environments (Van De Velde et al., 2023). Persistent anoxia in these coastal OMZ can lead to huge releases of sulfide (up to 13.7 mmol m^{-2} d^{-1}) and ammonium (up to 21.2 mmol m^{-2} d^{-1}) into the water column (Sommer et al., 2016).

The Santa Barbara Basin (SBB) is an example of one of these coastal OMZs that experiences seasonal deoxygenation. Drastic changes in water column oxygenation and seafloor redox

68   conditions drive complex changes in benthic biogeochemistry and microbiology, evidenced most

69   clearly by the development of thick, expansive mats of giant sulfur-oxidizing bacteria (GSOB)

70   on the SBB seafloor (Bernhard et al., 2003; Prokopenko et al., 2006; Valentine et al., 2016;

71   Kuwabara et al., 1999). A 2016 survey of the basin identified a vast GSOB mat spread over 1.6

72   contiguous km, confined between 487 and 523 km in the SBB depocenter where conditions were

73   anoxic but not depleted of NO_3^- (Valentine et al., 2016). These GSOB mats have been noted

74   previously in the SBB benthos, appearing at times of anoxia and disappearing when oxygen is

75   present in the bottom water (Reimers et al., 1996; Kuwabara et al., 1999). Similar GSOB mats

76   have been identified in other transiently deoxygenated OMZs such as the Peruvian/Chilean coast

77   (Sommer et al., 2016; Schulz et al., 1996; Zopfi et al., 2001; Høgslund et al., 2009). The

78   chemoautotrophic bacteria that constitute the bulk of GSOB mats (typically *Thioploca* and/or

79   *Beggiatoa*) utilize sulfide as an electron donor and O_2 or NO_3^- as a terminal electron acceptor

80   (Jørgensen and Nelson, 2004). Some GSOB can hyperaccumulate NO_3^- in cell vacuoles up to

81   500 mM (Fossing et al., 1995) and use this NO_3^- reserve to oxidize sulfide that diffuses from the

82   underlying sediment to perform their metabolism. (Huettel et al., 1996; Mußmann et al., 2003;

83   Sayama, 2001).
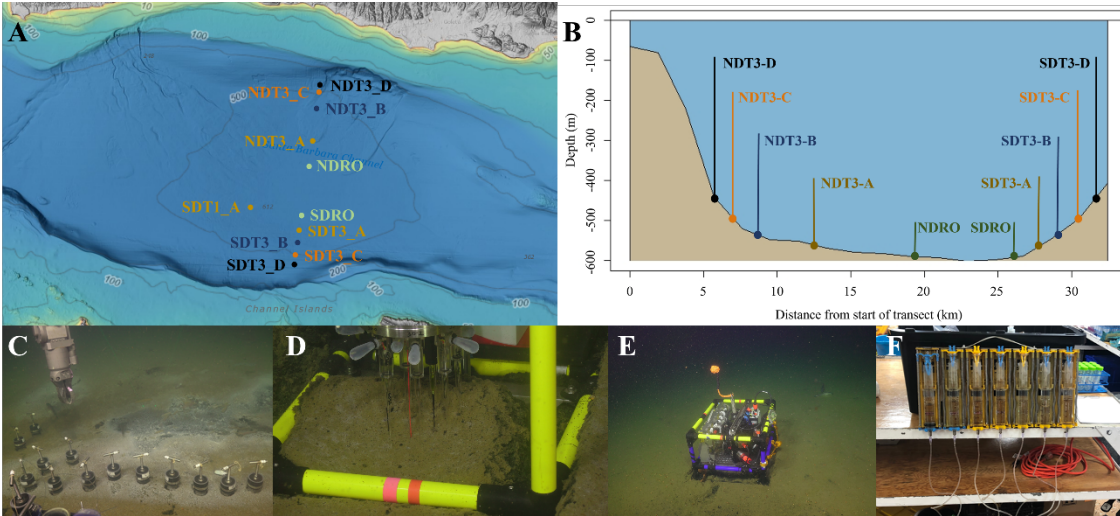
84

Figure 1. Maps of sampling locations in the Santa Barbara Basin and photographs of deployed equipment: (A) bathymetric map of the Santa Barbara Basin with locations of all sampled stations; (B) cross-section of the Santa Barbara Basin with locations of all sampled station; (C) sediment push coring with ROV arm; (D) sediment microprofiler; (E) benthic flux chamber; (F) closeup of a syringe system from a benthic flux chamber. The map in (A) was generated using the Bathymetric Data Viewer provided by the National Centers for Environmental Information.

The activity of GSOB mats contribute significantly to element cycling in benthic marine environments with large effects on biogeochemical conditions in the bottom water. Isotopic measurements of $^{15}N/^{14}N$ and $^{18}O/^{16}O$ from NO_3^- in the SBB water column suggest that benthic organisms are responsible for approximately 75% of the total NO_3^- reduction in the SBB (Sigman et al., 2003). Other studies found that GSOB mats inhibit the diffusion of NO_3^- into sediments via hyper-accumulation in vacuoles thereby creating conditions ideal for bacterial heterotrophic sulfate reduction beneath them (Fossing et al., 1995; Zopfi et al., 2001). These studies suggest that GSOB mats in the SBB may be responsible for the majority of NO_3^- consumption in the basin rather than water-column microbes. Additionally, GSOB mats have been reported to deplete NO_3^- via dissimilatory nitrate reduction to ammonia (DNRA) in the anoxic bottom water of the Peruvian OMZ (Dale et al., 2016) and in the hypoxic transition zone

106 in the Eastern Gotland Basin of the Baltic Sea (Noffke et al., 2016). By contrast, benthic

107 microbial communities in the hypoxic (42 μM) Mauritanian OMZ perform canonical

108 denitrification instead (Dale et al., 2014). The contrast between the Peruvian and Mauritanian

109 OMZ suggests that bottom- water anoxia triggers the appearance of GSOB mats, and that DNRA

110 is more prevalent where GSOB mats are present.

111

112 The rapid accumulation and consumption of NO_3^- by GSOB mats has ramifications for the redox

113 conditions in the sediment underneath. The depletion of NO_3^- and shallowing of the nitracline

114 could promote high rates of sulfate reduction in the sediment underneath the GSOB mat. In

115 return, the sulfate reduction zone exists close to the sediment-water interface, providing the

116 GSOB mat with readily accessible sulfide. If a metabolic feedback loop is then established

117 between sulfur-oxidizing bacteria at the sediment-water interface and sulfate-reducing bacteria in

118 the sediment, increased NO_3^- loss from the water column and spreading of sulfidic conditions in

119 SBB sediment is expected. With these mats being potentially crucial to nitrogen and sulfur

120 cycling in sediments underlying OMZs, their biogeochemical transformations and ergo effect

121 upon basin redox conditions are critically important to understanding element cycling in the

122 SBB. Such gained knowledge would have additional benefits for predicting biogeochemical

123 feedbacks to the projected expansion of oceanic oxygen deficiency, in the SBB and in OMZs

124 more general, as a result of global change (Stramma et al., 2008).

125

126 Utilizing in-situ technologies, sediment porewater extraction, solid phase analyses, and

127 radiotracer techniques, this study aims to answer the following overarching questions: (1) Which

128 environmental conditions initiate and sustain the proliferation of GSOB mats? (2) Which

129   biogeochemical transformations occur in the sediment underneath these mats? (3) What role do

130   the mats play in the increasingly prevalent anoxic and nitrate-depleted condition found in the

131   SBB? These investigations represent the first basin-wide geochemical characterization of the

132   Santa Barbara Basin which hosts the largest as-of-yet mapped GSOB mat in the world's oceans.

133   It is the first suite of in-situ flux measurements carried out in the SBB, which is unique to other

134   heavily studied marine settings (e.g., Eastern Gotland Basin, Peruvian upwelling zone) in that it

135   is an oceanic basin within an upwelling zone. The results presented here also provide

136   geochemical context for a number of other related investigations in the SBB (Robinson et al.,

137   2022; Xuefeng Peng et al., 2023; Peng et al., 2023) as well as the first measurements in a multi-

138   year study of biogeochemical changes in response to warming waters and increased stratification

139   on the California coast.

2. Materials and Methods

2.1 Study Site

The Santa Barbara Basin (SBB) is a coastal basin in the California Borderland with an approximate maximum depth of 600 m characterized by a seasonally anoxic water column (Sverdrup and Allen, 1939; Sholkovitz and Gieskes, 1971). The transform boundary along the California Borderland heavily affects the geomorphology of basins in this region; these basins become twisted as the plates rub against each other and form a series of "bathtubs" blocked by sills and seamounts off the coast of California. The SBB is bordered by the California coast in the north, the Channel Islands in the south, the Santa Monica basin to the east, and the Arguello Canyon to the west. A sill to the west of the basin at around 475 m depth (Fig. 1) prohibits most water transfer between the Santa Lucia Slope and the deeper waters of the SBB (Sholkovitz and Gieskes, 1971). The highly productive surface waters in the basin provide ample organic matter to the basin's water column, encouraging strong remineralization processes below the euphotic zone, which can induce anoxia below the sill depth, with typically less than 1 µmol O_2 L^{-1} (Sholkovitz, 1973; Emery et al., 1962; Thunell, 1998; Emmer and Thunell, 2000). Benthic faunal distribution within the basin is tightly correlated with this sill depth and related oxygen conditions; below the sill, the sea snail *Alia permodesta* is the most commonly found benthic fauna, while sea stars, sea urchins, and other echinoderms increase in density above the sill (Myhre et al., 2018). During upwelling events (usually in Spring), oxygenated waters from the California Current spill over the western sill and ventilate the SBB, reportedly increase bottom water oxygen concentrations to approximately 20 µmol O_2 L^{-1} (Goericke et al., 2015). SBB water-column oxygen and nitrogen concentrations have been evaluated through a longitudinal survey by the California Cooperative Oceanic Fisheries Investigations (Calcofi) with data

163   starting in the 1950's . The data collected by this survey shows increasing durations of anoxia

164   and fixed nitrogen loss in the basin with the SBB becoming completely nitrate-depleted below

165   the sill at least three times between 2012 and 2017 (https://calcof.iorg/data/).

166

167   **2.2 Benthic sediment sampling and instrument deployment**

168   Sediment samples were taken between 30 October and 11 November 2019 during an expedition

169   aboard the research vessel *(R/V) Atlantis* equipped with the remote operated vehicle (ROV)

170   Jason. Samples were taken at stations along a bimodal, north-south transect through the

171   depocenter of the SBB, as well as one station on a separate transect. Details of sampling stations

172   can be seen in Fig. 1A and 1B. Briefly, depocenter stations are labeled as NDRO and SDRO

173   (northern and southern depocenter radial origin, respectively). The remaining stations are named

174   for the cardinal direction (north vs. south) and the transect number (e.g., SDT1-A is on transect 1

175   while SDT3-A is on transect 3). As station depth decreases, the alpha suffix increases (e.g.,

176   NDT3-A is deeper than NDT3-B, etc.).

177

178   ROV Jason conducted sediment push coring and deployed automated benthic flux chambers

179   (BFC) and microprofilers at each station. Bottom water oxygen concentration was determined

180   using an Aanderaa 4831 oxygen optode (Aanderaa Instruments, Bergen, Norway) installed on

181   the ROV. Optical modems (Luma 250LP, Hydromea, Renens, Switzerland) installed on the ROV

182   and the BFC and microprofilers were used to transmit deployment settings and start/terminate

183   measurements of the instruments. Multiple push cores (polycarbonate, 30.5 cm length, 6.35 cm

184   inner diameter) per sampling station were retrieved during ROV Jason deployments (Fig. 1C).

185   Replicate cores from each station were transferred to an onboard 6°C cold room upon recovery

186 aboard the ship and subsampled for either solid phase analyses, porewater geochemistry, or

187 radiotracer experiments.

188

189 **2.3 Sediment Core Sub-Sampling**

190 Two replicate ROV push cores that were collected near each other at each station were processed

191 under a constant argon flow to protect redox-sensitive species. Cores were sectioned in 1-cm

192 increments up to 10 cm followed by 2-cm increments. Note, sediments from the NDT3-B station

193 were sliced in 2-cm increments. Sediment subsections were transferred into argon-filled 50-mL

194 conical centrifuge tubes. Sediment samples were centrifuged at 2300 x g for 20 minutes. The

195 centrifugate was subsampled unfiltered as fast as possible (to avoid contaminations with oxygen)

196 for porewater analyses. Solid phase cores were sectioned similar to porewater cores and sub-

197 sampled for sediment density, porosity, and organic matter content. A 10 mL cut-off plastic

198 syringe was used to collect 6 mL of sediment into pre-weighed plastic vials (15 mL snap-cap

199 vials) and stored in the dark at 4°C for sediment porosity and density analysis. Two-mL

200 microcentrifuge tubes were filled with sediment from each depth interval and stored at -30°C for

201 sediment organic matter analyses. One ROV push core per station was sub-sampled with a

202 miniaturized push core (length 20 cm, inner diameter 2.6 cm) and taken immediately to the

203 shipboard radioisotope van for radiotracer experiments (see section 2.5).

204

205 **2.4 Sediment Porewater Geochemistry**

206 Concentrations of porewater sulfide (Cline, 1969), NH_4^+, PO_4^{3-}, and Fe^{2+} (Grasshoff et al., 1999)

207 were determined shipboard with a Shimadzu UV-Spectrophotometer (UV-1800). Detection

208 limits for sulfide, NH_4^+, PO_4^{3-}, and Fe^{2+} were 1 μM. Subsamples (2 mL) for porewater NO_3^- and

209   NO_2^- concentrations were stored in 2-mL plastic vials with an O-ring, frozen shipboard at -30°C

210   and analyzed back at the home laboratory on the same spectrophotometer using the method

211   following (García-Robledo et al., 2014). The detection limit for NO_3^- and NO_2^- was 0.5 µM.

212   Samples for porewater DIC were preserved shipboard with 5 µL saturated HgCl in headspace

213   free glass vials and stored at 4°C for later analysis following (Hall and Aller, 1992). DIC

214   detection limit was 0.1 mM. Total alkalinity was determined shipboard using direct titration of

215   500 µL of pore water with 0.01M Titrisol® HCl (Pavlova et al., 2008). The analysis was

216   calibrated using IAPSO seawater standard, with a precision and detection limit of 0.05 meq L^{-1}.

217   Subsamples (1 mL) for sulfate and chlorinity were stored in 2-mL plastic vials with an O-ring,

218   frozen shipboard at -30°C and later measured in the lab using a Metrohm 761 ion chromatograph

219   with a methodological detection limit of 30 µM (Dale et al., 2015).

220

221   **2.5 Solid Phase Analyses**

222   Porosity/Density samples were collected in pre-weighed plastic vials and dried at 50°C for up to

223   96 hr until the dry weight was stable. Sediment porosity was calculated by taking the difference

224   between wet and dry sediment weight and divided by the volume of the wet sediment. Sediment

225   density was calculated by dividing the wet sediment weight by its volume. Treatment of

226   sediment subsamples for total organic carbon (TOC), total organic nitrogen (TON), and organic

227   carbon isotope composition ($\delta^{13}C$) were modified from (Harris et al., 2001) and sent to the

228   University of California Davis Stable Isotope Facility for analysis using Elemental Analyzer –

229   Isotope Ratio Mass Spectrometry. TOC and TON were calculated based on the sample peak area

230   corrected against a reference material (alfalfa flour). Limit of quantification based on peak area

231   was 100 µg C with an uncertainty of ± 0.2 ‰ for $\delta^{13}C$.

232

2.6 Sulfate Reduction

To determine ex-situ microbial sulfate reduction rates, whole round sub-cores were injected with 10 µL carrier-free ^{35}S-Sulfate radiotracer (dissolved in water, 200 kBq, specific activity 37 TBq mmol^{-1}) into pre-drilled, silicon-filled holes at 1-cm increments according to (Jørgensen, 1978). These sub-cores were incubated at 6°C in the dark for 6-8 hours. Incubations were stopped by slicing sediment cores in 1-cm increments into 50-mL centrifuge tubes filled with 20-mL zinc acetate (20% w/w) and frozen at -20°C until analysis at the land-based laboratory. Microbial activity in controls was terminated with zinc acetate (20 mL of 20% w/w) before the addition of radiotracer and subsequent freezing. Lab-based analysis of sulfate reduction rates were determined following the cold-chromium distillation procedure (Kallmeyer et al., 2004).

243

2.7 Benthic In-Situ Investigations

Per station, one to three microprofiler (Fig. 1D) and three BFC (Fig. 1E) deployments were carried out by the ROV Jason at the seafloor. Construction, deployment and operation of automated microprofilers and BFCs followed those described in (Treude et al., 2009). The microprofiler deployed in this study represents a modified, miniaturized version of the instrument described in (Gundersen and Jørgensen, 1990) that was constructed specifically for use by ROV. Microprofilers were outfitted with three O_2-microelectrodes (Glud et al., 2000), two pH-microelectrodes (Revsbech and Jørgensen, 1986), two H_2S-microelectrodes (Jeroschewsky et al., 1996), and one conductivity sensor to determine the position of the sediment-water interface relative to the tips of the microelectrodes. Concentrations of oxygen

254   and sulfide, as well as pH were each calculated from microelectrode readings and averaged for

255   the respective sites where replicates existed.

256

257   The BFC consisted of a frame equipped with a cylindrical polycarbonate chamber (inner

258   diameter = 19 cm) with its lower portion sticking out of the frame. The upper side of the

259   chamber was closed by a lid containing a stirrer (Type K/MT 11, K.U.M., Kiel, Germany),

260   oxygen optodes (Type 4330, Aanderaa Data Instruments, Bergen Norway and Hydroflash,

261   Contros/Kongsberg Maritime, Kongsberg, Norway), a conductivity sensor (type 5860, Aanderaa

262   Data Instruments), and a valve. Prior to insertion into the sediments, the chambers were held

263   upside down by the ROV manipulating arms within approximately 10 m of the seafloor and

264   moved back and forth to make sure that water from shallower depth that may have been trapped

265   was replaced by bottom water. Chamber incubations lasted between 240 and 390 minutes. Each

266   BFC was outfitted with a custom-built syringe sampler containing seven syringes that were

267   connected by tubes to sampling ports in the upper wall of the chambers (Fig. 1F): one injection

268   syringe and six sampling syringes that were fired at regular time intervals over the time course of

269   the deployment. The injection syringe contained de-ionized water and the reduction in salinity in

270   the overlaying water after salinity readings stabilized (i.e., full mixing was achieved) 10-30 min

271   after injection was used to determine BFC volumes (Kononets et al., 2021). Samples obtained

272   from the overlaying water of the BFC were examined for the same geochemical constituents as

273   described above (section 2.4). Benthic fluxes of NO_3^-, NH_4^+, PO_4^{3-}, and Fe^{2+} were calculated as

274   follows:

275

276    $J = \frac{\Delta c}{\Delta t} * \frac{V}{A}$ (EQ # 2)

277

278   Where J is the flux in mmol m^{-2} d^{-1}, ΔC is the concentration change in mmol m^{-3}, Δt is the time

279   interval in d, V is the overlying water volume in m^3, and A is the surface area of the sediment

280   covered by the benthic flux chamber in m^2. An average flux within BFC's was calculated for

281   stations of similar depth. One chamber per site contained ^{15}N-NO_3^- in the injection syringe for in-

282   situ nitrogen cycling experiments. Results are reported from two of these chambers (SDRO and

283   NDT3-D) and all ^{15}N-NO_3^- chambers were excluded from benthic flux calculations (see next

284   section).

285

286   **2.8 In Situ ^{15}N Incubations**

287   Two hundred μmol of ^{15}N-labeled potassium nitrate (99% ^{15}N; Cambridge Isotopes) was injected

288   into the ^{15}N incubation chamber at each site to obtain a final concentration of ~50 – 100 μM ^{15}N-

289   labeled nitrate. Nitrate was amended at this level to prevent its depletion before the last sampling

290   time point (Valentine et al., 2016). Samples for $\delta^{15}N$ analysis were preserved by filling a pre-

291   vacuumed 12-ml exetainer vial with 0.1 ml 7M zinc chloride as a preservative. Another aliquot

292   (~12 ml) of seawater for ammonium isotope analysis (see section 2.7.2) was filtered through 0.2

293   μm syringe filters and stored frozen. Prior to analyzing the samples in 12-ml exetainer vials, 5

294   mL of sample was replaced with ultra-high purity helium to create a headspace. The

295   concentration and $\delta^{15}N$ of dissolved N_2 and N_2O was determined using a Sercon CryoPrep gas

296   concentration system interfaced to a Sercon 20-20 isotope-ratio mass spectrometer (IRMS) at the

297   University of California Davis Stable Isotope Facility.

298

299   **2.9 Ammonium Isotope Analyses**

300 The production of $^{15}NH_4^+$ in seawater samples was measured using a method adapted from

301 (Zhang et al., 2007) and described previously by (Peng et al., 2016). In brief, NH_4^+ was first

302 oxidized to NO_2^- using hypobromite (BrO^-) and then reduced to N_2O using an acetic acid-azide

303 working solution (Zhang et al., 2007). The $\delta^{15}N$ of the produced N_2O was determined using an

304 Elementar Americas PrecisION continuous flow, multicollector, isotope-ratio mass spectrometer

305 coupled to an automated gas extraction system as described in (Charoenpong et al., 2014).

306 Calibration and correction were performed as described in (Bourbonnais et al., 2017). The

307 measurement precision was ±0.2 ‰ for $\delta^{15}N$. Depending on the in-situ ammonium

308 concentration, the detection limit for total NH_4^+ production rates ranged between 0.006 and

309 0.0685 mmol m^{-2} d^{-1}.

310

3. Results

3.1 Bottom water conditions

O_2 and NO_3^- concentrations in the bottom water along the transects can be seen in Table 1. O_2 concentrations below detection as determined by the ROV sensor could in some cases be considered to represent anoxia (0 μM O_2) based on a set of different analytical methods (see discussion section 4.1). Bottom water solute concentrations (as defined by the average T_0 concentration in BFC at each site) can be seen in Suppl. Figs. 1-4. Bottom water NO_3^- concentrations roughly decreased with station depth (e.g., 28 μM at NDT3-D vs. 19 μM at NDRO). Bottom water NO_2^- concentrations were below detection at all stations. Bottom water NH_4^+ concentrations were 9 μM at NDRO and 13 μM at SDRO and below detection in shallower stations. Bottom water PO_4^{3-} concentrations roughly increased with increasing basin depth (e.g., 2 μM at SDT3-D vs. 7 μM at SDRO). Finally, Fe^{2+} was 2 and 5 μM at the NDRO and SDRO stations, respectively and below detection at all shallower stations.

3.2 Sediment characteristics

Photographs of sediment cores with a depth scale are shown below Table 1. Sediment colors were classified according to (Hossain et al., 2014). Cores from the shallowest (D) stations were uniformly reddish in color with small pockets of black. The sediment color changed with station depth, transitioning from a reddish color in the shallowest stations to predominantly black with reddish laminations at the depocenter stations. The band of black sediment appeared at approx. 8 cm sediment depth in the C-station cores and became progressively more ubiquitous with station depth. Notably, NDT3-C sediment (Table 1B) contained black bands from approx. 6-14 cm sediment depth, while SDT3-C sediment (Table 1J) had a much narrower band around 8-10 cm.

334   Sediment cores from shallower stations (D and C stations) contained signs of bioturbation (e.g.,

335   u-shaped burrows) and, in some cases, contained visible macrofauna, such as polychaetas and

336   mollusks. Deeper in the basin (A and depocenter stations) no signs of bioturbation were detected,

337

338 **Table 1.** Station details and photos of representative ROV push cores taken at each station. Mat presence (Y =
339 yes, N = no) was determined visually. Station water depth and oxygen concentration were determined by sensors
340 attached to ROV Jason (bdl = below detection limit (<3 µM O$_2$). Anoxia was confirmed by additional methods
341 (see discussion section 4.1). Latitude and longitude were determined by triangulation between the ROV and the
342 ship. Bottom water nitrate concentration was derived from an average of benthic flux chamber nitrate
343 measurements at time 0 for each station (chambers with no calculatable flux and ^{15}N-nitrate addition excluded).
344 Note, benthic flux chambers were not deployed at SDT1-A. Photographs show the sediment-water interface
345 (SWI; top part) and each sediment core in full length (lower part).
346

Parameter	NDT3-D	NDT3-C	NDT3-B	NDT3-A	NDRO	SDRO	SDT1-A	SDT3-A	SDT3-B	SDT3-C	SDT3-D
Mat Present	N	N	N	Y	Y	Y	Y	Y	N	N	N
Depth (m)	447	498	537	572	580	586	573	571	536	494	447
Latitude (°)	34.363	34.353	34.333	34.292	34.262	34.201	34.212	34.184	34.168	34.152	34.142
Longitude (°)	-120.015	-120.016	-120.019	-120.026	-120.031	-120.044	-120.116	-120.047	-120.053	-120.050	-120.052
Oxygen (µM)	8.7	5.2	12.2	9.2	0.0	0.0	0.0	0.0	1.8	3.1	9.6
Nitrate (µM)	27.3	26.0	11.5	24.4	18.5	9.9		20.4	20.6	16.3	28.0
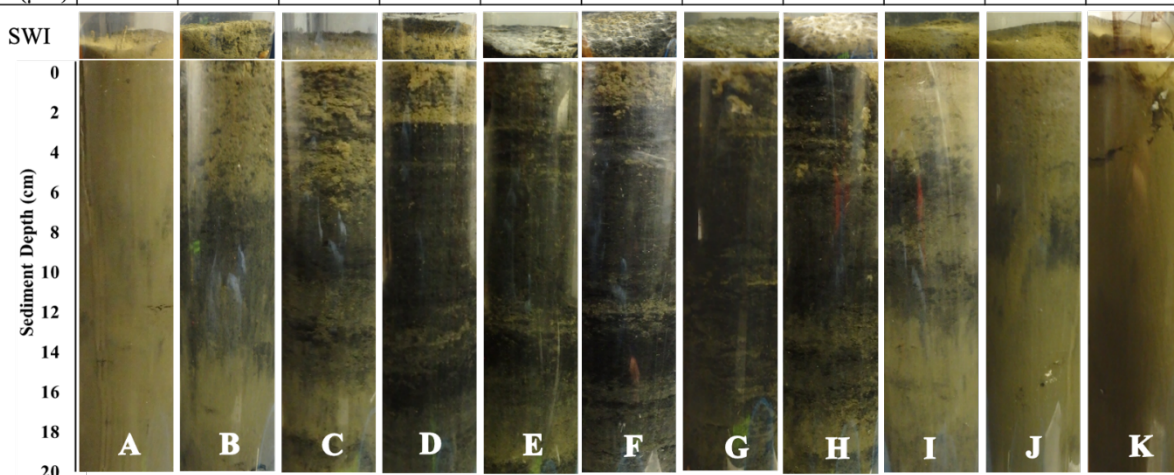
347
348

349   and the sediment-water interface was colonized by patches of white GSOB mats. Spherical cells

350   (given the moniker 'ghost balls') were found mixed amongst giant sulfur bacteria filaments

351   within the top 0-1 cm of sediment at NDRO (Suppl. Fig. 7). These unknown species had similar

352   morphological characteristics to the species *Thiomargarita namibiensis* (Schulz et al., 1999;

353   Schulz and Schulz, 2005) containing a translucent cell with sulfur granules giving them a ghostly

354 white appearance. A small sample of cells (n = 8) were measured, featuring diameters between

355 48.0 and 99.6 μm, amounting to an average biovolume of 2.5×10^5 μm^3, compared to *T.*

356 *namibiensis* with a cell diameter usually between 100-300 μm (Schulz et al., 1999).

357
358 **Table 2.** Sediment solid phase data: porosity, density, total organic carbon (TOC), total organic nitrogen (TON),
359 C:N ratio, and δ13C. All data were averaged for the top 0-19 cm sediment, except NDT3-C (17 cm), NDT3-A
360 (11 cm) and SDRO (7 cm), where the core length was shorter. Integrated sulfate reduction rates (iSRR) were
361 integrated over 0-14 cm sediment depth. No sulfate reduction rates are available for NDT3-B, SDT3-A, and
362 SDT3-B; rates were not integrated for SDRO due to missing surface samples.
363

Parameter	NDT3-D	NDT3-C	NDT3-B	NDT3-A	NDRO	SDRO	SDT1-A	SDT3-A	SDT3-B	SDT3-C	SDT3-D
Porosity	0.79 ± 0.03	0.81 ± 0.04	0.86 ± 0.04	0.88 ± 0.03	0.88 ± 0.04	0.87 ± 0.03	0.88 ± 0.03	0.86 ± 0.04	0.85 ± 0.04	0.82 ± 0.04	0.78 ± 0.04
Density	1.21 ± 0.07	1.16 ± 0.08	1.06 ± 0.08	1.05 ± 0.04	1.06 ± 0.03	1.04 ± 0.03	1.11 ± 0.23	1.05 ± 0.05	1.12 ± 0.06	1.22 ± 0.05	1.22 ± 0.03
TOC (%)	2.9 ± 0.5	2.5 ± 0.5	3.6 ± 0.5	3.1 ± 0.4	3.3 ± 0.4	3.5 ± 0.4	4.5 ± 0.5	3.2 ± 0.0	3.6 ± 0.6	3.6 ± 0.8	3.3 ± 0.5
TON (%)	0.3 ± 0.1	0.5 ± 0.1	0.4 ± 0.1	0.4 ± 0.1	0.4 ± 0.0	0.4 ± 0.1	1.0 ± 0.1	0.4 ± 0.0	0.4 ± 0.1	0.4 ± 0.1	0.4 ± 0.1
C:N Ratio	8.9 ± 0.2	8.7 ± 0.5	8.5 ± 0.5	8.2 ± 0.2	8.2 ± 0.4	8.0 ± 0.2	8.6 ± 0.8	8.3 ± 0.6	8.3 ± 0.3	8.7 ± 0.3	8.5 ± 0.2
δ^{13}C (‰)	-22.4 ± 0.3	-22.4 ± 0.4	-22.2 ± 0.4	-22.1 ± 0.2	-22.1 ± 0.2	-22.0 ± 0.3	-21.3 ± 0.7	-22.1 ± 0.4	-22.0 ± 0.2	-21.9 ± 0.2	-22.0 ± 0.1
Integrated SRR (mmol m^{-2} d^{-2})	2.9	3.8		2.7	4.1		2.9			1.7	1.9

367 B station cores contained sporadic GSOB filaments slightly deeper in the sediment (approx. 2-4

368 cm sediment depth). Sediment solid phase parameters (averaged over the entire sediment core

369 depth) can be seen in Table 2. Average sediment porosity increased with basin depth (e.g., from

370 0.79 at NDT3-D to 0.88 at NDRO). TOC, TON, the C/N ratio, and the δ^{13}C isotopic signature of

371 organic carbon remained relatively constant (2.5 – 4.5%, 0.1 – 0.4%, 8.0 – 8.7 and 21.3 –

372 22.4 ‰, respectively) over all stations.

373

3.3 Sediment porewater geochemistry

375 Total alkalinity (Figs. 2 A-E & 3 A-F) increased steadily with sediment depth at all stations

376 starting with, on average, 2.4 mM in the core supernatant reaching a maximum at the respective

377 deepest sediment sample (20 cm). Porewater alkalinity and DIC also increased with basin depth

378   (Figs. 2 A-E & 3 A-F) indicating that total alkalinity was dominated by the carbonate system.

379   Porewater DIC was, on average, 2.2 mM in the core supernatant and reached maximum

380   concentrations at the deepest sediment depth (20 cm) at most stations.

381

382   Porewater PO_4^{3-} profiles (Figs. 2 A-E & 3 A-F) were markedly different between the depocenter

383   and shallower C and D stations. Porewater PO_4^{3-} concentrations in the depocenter and A stations

384   generally increased with sediment depth but several profiles (NDT3-C, NDT3-A, SDRO, SDT1-

385   A) remained unchanged or decreased deeper in the sediment (starting at approx. 10 cm). The

386   profiles in C and D stations showed a peak in PO_4^{3-} concentrations near the sediment-water

387   interface, particularly in the northern basin. Below 2 cm, PO_4^{3-} decreased with sediment depth,

388   but sometimes showed a second small peak deeper in the sediment (12-14 cm at NDT3-D and

389   10-12 cm at SDT3-D).

390

391   Porewater NH_4^+ concentrations (Figs 2 & 3 A-E) showed trends often similar to alkalinity and

392   DIC; NH_4^+ concentrations increased downcore and were higher at depocenter than at D stations

393   (e.g., 370 and 91 µM at 20 cm for SDRO and SDT3-D, respectively). Porewater NO_2^- (Suppl.

394   Table 1) and NO_3^- (Figs. 2 F-J & F G-L) concentrations were at or near zero below 2 cm at every

395   station, except at SDRO and NDT3-A where large peaks in NO_3^- (376 and 81 µM, respectively)

396   and NO_2^- (37 and 5 µM, respectively) occurred in the top 1 cm.

397

398   Porewater Fe^{2+} concentrations (Figs. 2 F-J & 3 G-L) were several orders of magnitude higher at

399   shallower D-stations (max. 722 and 395 µM at NDT3-D and SDT3-D, respectively) compared to

400   depocenter stations (max. 13 and 51 µM at NDRO and SDRO, respectively). NDT3-C porewater

401   Fe^{2+} concentration (Fig. 2G) peaked in the top 1 cm of sediment (similar to deeper stations)

402   while SDT3-C porewater Fe^{2+} concentration (Fig. 3H) peaked around 5-cm sediment depth. Fe^{2+}

403   concentrations reached a max. at 0-2 cm and declined sharply with depth in depocenter and A-

404   station sediment. Northern basin sediment was similar, but the decline in Fe^{2+} below 0-2 cm was

405   less pronounced.

406

407   Maximum porewater sulfide concentrations (Figs. 2 F-J & 3 G-L) were several orders of

408   magnitude lower at the shallower D-stations (5 and 4 µM at NDT3-D and SDT3-D, respectively)

409   compared to A stations (350 and 148 µM at NDT3-A and SDT1-A, respectively). Unlike Fe^{2+},

410   peaks in sulfide concentration occurred deeper in the sediment (e.g., below 5 cm depth at A

411   stations). Porewater sulfate concentrations (Figs. 2 K-O & 3 M-R) decreased slightly with depth,

412   but never reached values below 20 mM at any station.

413

414   **3.4 In-situ microprofiling**

415   Microprofiler O_2 and sulfide measurements are shown in Fig. 4. Oxygen was rapidly consumed

416   within the first 0-1 cm of sediment at every station where O_2 was detected in the bottom water

417   (i.e., at all stations except NDRO, which showed no positive signal of oxygen in the water

418   compared to the sediment; note that no oxygen profile is available for SDRO). Sulfide

419   concentrations from microsensors showed similar trends to spectrophotometric measurements,

420   albeit with different absolute values (below detection in shallower B-, C- and D-stations that

421   lacked mats and >1,000 µM at A- and depocenter stations). Microprofiler pH (Fig. 4) was near

422   7.5 in the bottom water at all stations, and slowly decreased to near 7.0 in the lower parts (3-5

423 cm) sediment at most stations except NDT3-C and SDT3-B. pH at 2.5 cm at SDT3-B reached

424 6.77, which was the lowest observed during this expedition.

425
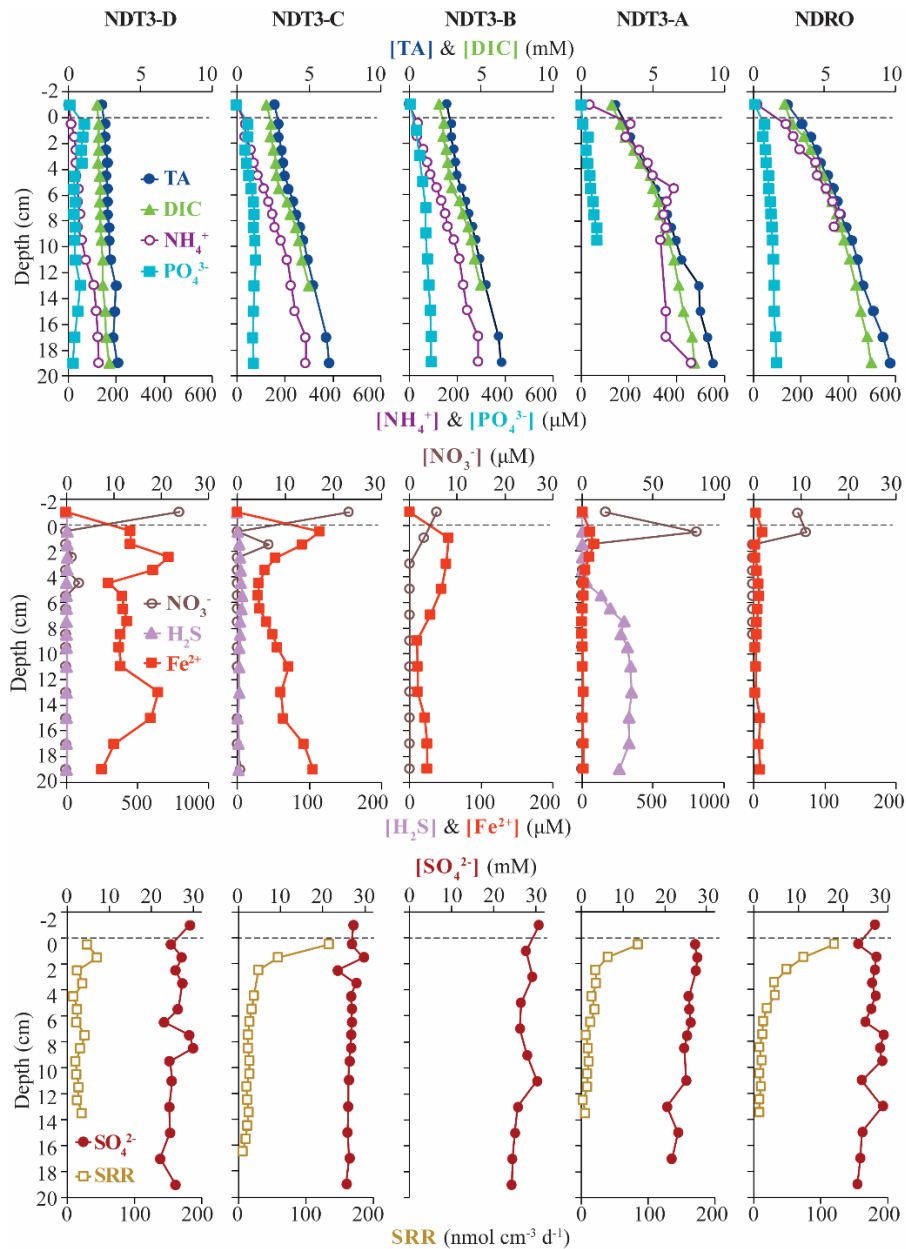
426
427 **Figure 2.** Biogeochemical data from ROV sediment push cores collected at stations on the northern transect
428 (NDT3) and in the northern depocenter (NDRO): total alkalinity (TA), dissolved inorganic carbon (DIC),
429 ammonium (NH_4^+), phosphate (PO_4^{3-}) in the first row; nitrate (NO_3^-), total sulfide (sulfide), and iron (II) (Fe^{2+})
430 in the second row; sulfate (SO_4^{2-}) and bacterial sulfate reduction rate (SRR) in the third row. Data analyzed from
431 sediment core supernatant are plotted at -1 cm sediment depth; the dotted line connotes the sediment-water
432 interface. Note the change in scale on the primary x-axis in panel I and the change in scale of the secondary x-
433 axis in panels F and I. No spectrophotometric sulfide data is available for NDRO and NDT3-B and no SRR data
434 is available for NDT3-B. For station details see Fig. 1 and Table 1.

435

436
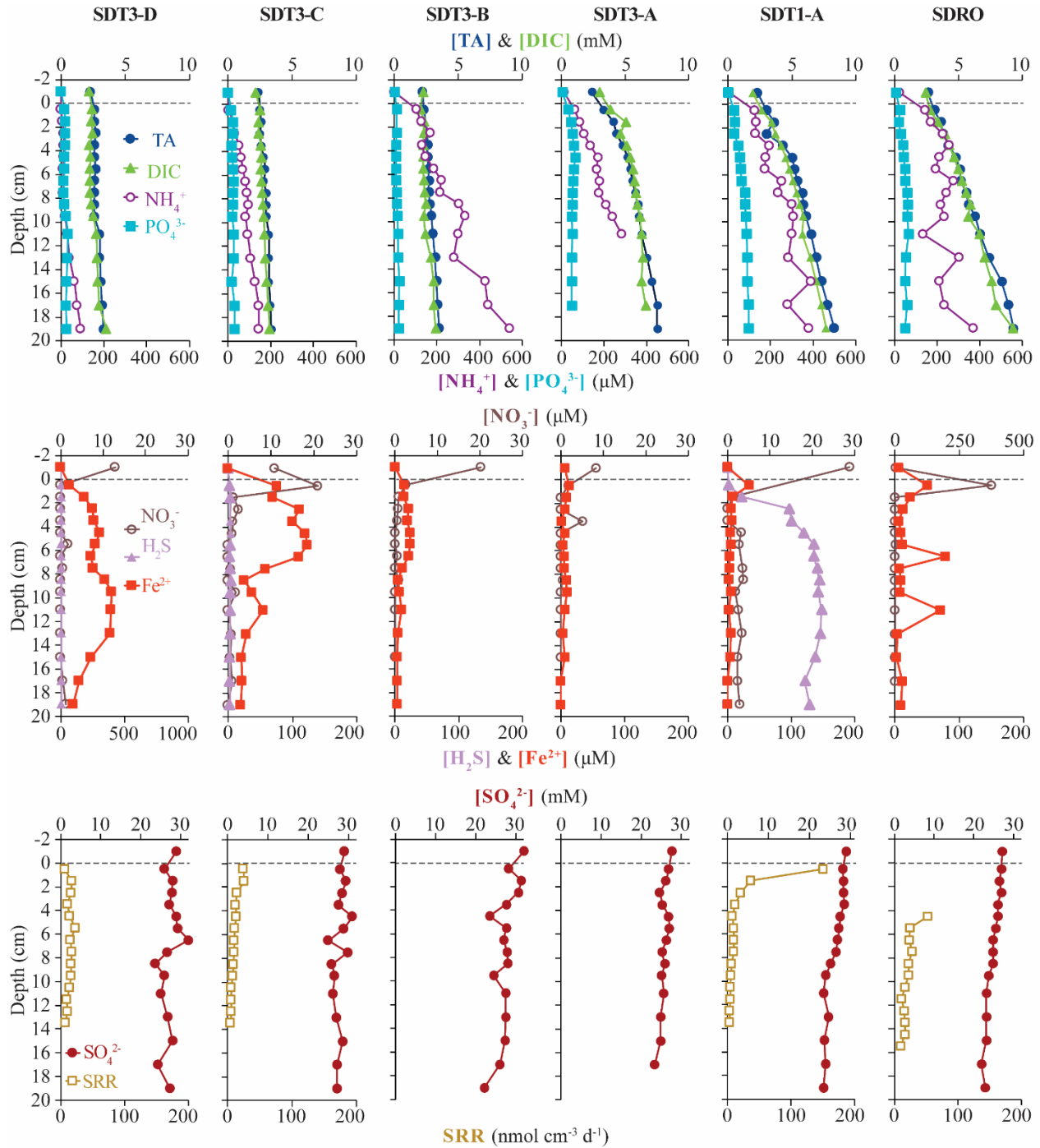
Figure 3. Biogeochemical data from ROV sediment push cores collected at stations on the two southern transects (SDT1 and SDT3) and the southern depocenter (SDRO): total alkalinity (TA), dissolved inorganic carbon (DIC), ammonium (NH_4^+), phosphate (PO_4^{3-}) in the first row; nitrate (NO_3^-), total sulfide (sulfide), and iron (II) (Fe^{2+}) in the second row; sulfate (SO_4^{2-}) and bacterial sulfate reduction rate (SRR) in the third row. Data analyzed from sediment core supernatant are plotted at -1 cm sediment depth; the dotted line connotes the sediment-water interface. Note the change in scale on the primary x-axis in panel L and the change in scale of the secondary x-axis in panel G. No sulfide nor SRR data are available for SDT3-B and -A; spectrophotometric sulfide and the top 0-4 cm of SRR data are not available for SDRO. For station details see Fig. 1 and Table 1.

445

446
447
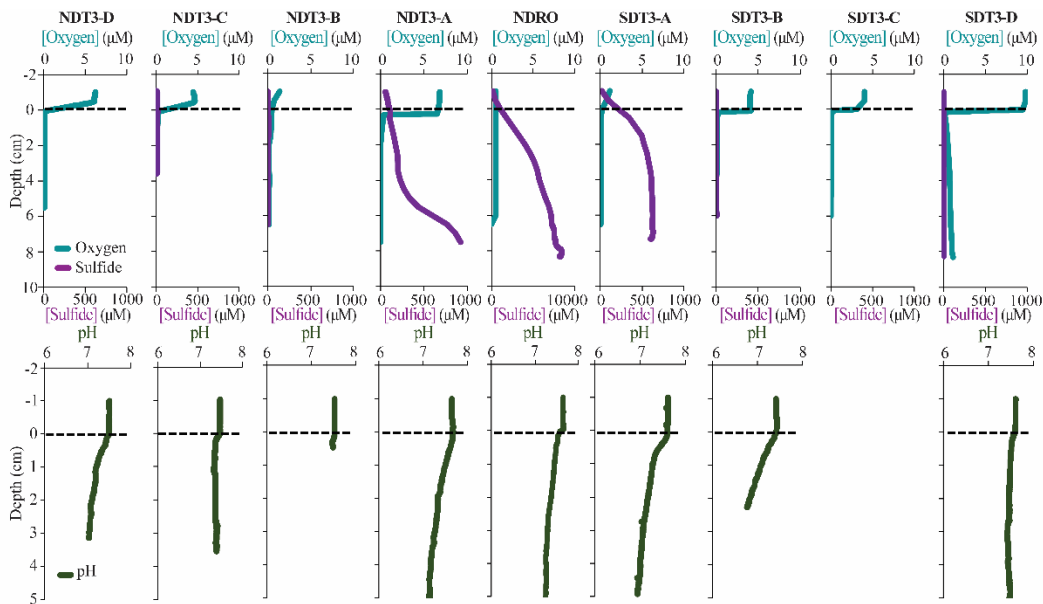
448
449
450 **Figure 4.** In-situ sediment microprofiler results for all stations (except SDT1-A and SDRO): oxygen (O_2) and
451 total sulfide (sulfide) concentration in the first row; pH profiles in the second row. Note the change in scale on
452 the secondary x-axis for NDRO sulfide. Values determined in the overlying water are plotted at negative
453 sediment depths; the dotted line connotes the sediment-water interface.
454

3.5 In-situ fluxes of benthic solutes

456 NO_3^-, NH_4^+, PO_4^{3-}, and Fe^{2+} flux measured in the BFC revealed different patterns of uptake and

457 release from the sediment throughout the basin (Fig. 5 and Suppl. Figs. 1-4). BFC O_2

458 concentrations were compromised by O_2 release from the chamber's polycarbonate walls, which

459 prevented an accurate calculation of O_2 fluxes from BFC sensor data. NO_3^- was consumed at all

460 stations as indicated by a negative flux (i.e., a flux into the sediment). On the contrary, benthic

461 release (i.e., a flux out of the sediment) was observed for all other analyzed solutes (NH_4^+, PO_4^{3-},

462 and Fe^{2+}), with the lowest fluxes in the shallow D and C-stations and highest fluxes in the

463 depocenter. Ammonium fluxes were the highest of all the determined solutes and showed the

464 largest difference between deep and shallow stations, with a flux of 1.6 mmol m^{-2} d^{-1} at NDT3-C

465 (there were no measurable NH_4^+ fluxes in D-station chambers) and reaching 11.1 ± 3.1 mmol m^{-2}

466 d^{-1} (n = 3) at the two depocenter stations. The depocenter ammonium flux far-outpaced the

467 concomitant flux of nitrate into depocenter sediments (-3.2 $\pm$ 0.7 mmol m^{-2} d^{-1}, n = 3). Iron and

468 phosphate fluxes were similar at depocenter stations (4.1 $\pm$ 0.7, n = 3, and 3.2 $\pm$ 0.7, n = 3, mmol

469 m^{-2} d^{-1}, respectively). Alkalinity and DIC concentrations from flux chambers (Suppl. Figs. 5 and

470 6) remained constant at all stations and thus no DIC flux was calculated. Results from BFCs

471 injected with ^{15}N-NO$_3^-$ at the SDRO and NDT3-D station are shown in Fig. 6. The rates of

472 denitrification, anammox, and N$_2$O production were higher at SDRO compared to NDT3-D.

473 ^{15}NH$_4^+$ production (DNRA) was one order of magnitude higher at the SDRO station (2.67 mmol

474 m^{-2} d^{-1}) compared to the NDT3-D station (0.14 mmol m^{-2} d^{-1}). DNRA accounted for a much

475 higher percentage of NO$_3^-$ reduction at SDRO (54.1%) than NDT3-D (13.3%).

476

477 **3.6 Sulfate reduction rates**

478 Vertical profiles of bacterial sulfate reduction as determined by the radioisotope technique

479 differed throughout the basin (Figs. 2 & 3). Peaks in sulfate reduction were seen in the top 0-1

480 cm of sediment at stations with a visible GSOB mat on the surface (120.2, 151.0, and 85.3 nmol

481 cm^{-3} d^{-1} at NDRO, SDT1-A, and NDT3-A, respectively). Sediments at most shallower basin

482 depths exhibited peaks slightly deeper in the sediment and of lower magnitude (25.5, 44.5, 22.5

483 nmol cm^{-3} d^{-1} at SDT3-C, NDT3-D, and SDT3-D respectively). NDT3-C had no visible GSOB

484 mats but exhibited a peak (133.7 nmol cm^{-3} d^{-1}) in sulfate reduction at 0-1 cm depth, similar to

485 deeper stations (e.g., NDRO in Fig. 2O), which differed from other shallow stations (e.g., SDT3-

486 C in Fig. 3N). The integrated sulfate reduction rate (0-14 cm depth) at NDRO (4.1 mmol m^{-2} d^{-1})

487 was noticeably higher than most other stations with the exception of NDT3-C (3.8 mmol m^{-2} d^{-1})

488   (Table 2). NDT3-D and NDT3-C exhibited higher integrated rates (2.9 and 3.8 mmol m^{-2} d^{-1})

489   than their southern station counterparts SDT3-D and SDT3-C (1.9 and 1.7 mmol m^{-2} d^{-1}).

490
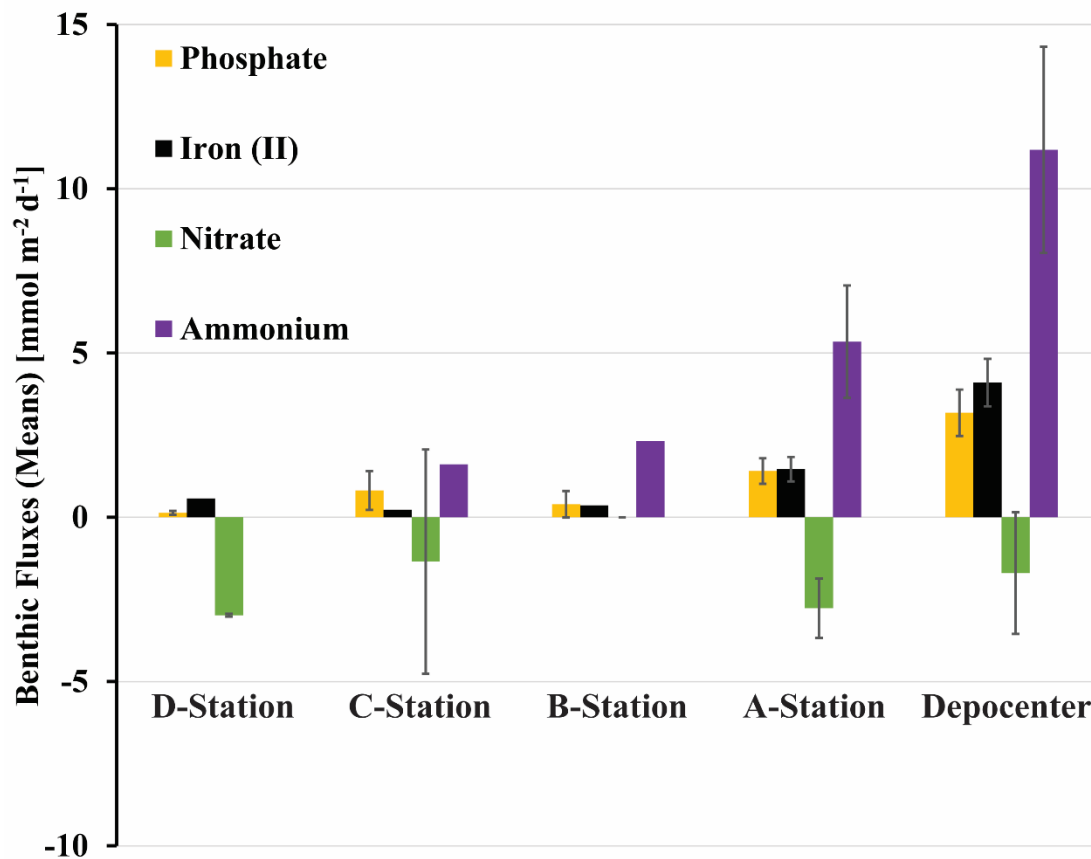
491
492
493   **Figure 5.** Benthic fluxes of solutes (positive flux = release from the seafloor; negative flux = uptake by the
494   seafloor) determined with in-situ benthic flux chambers. Rates were averaged for stations of same depth from
495   the northern and southern transect and the depocenter (NDRO and SDRO). Note, giant sulfur-oxidizing bacterial
496   mats were found at depocenter and A-stations. Error bars represent standard errors.
497
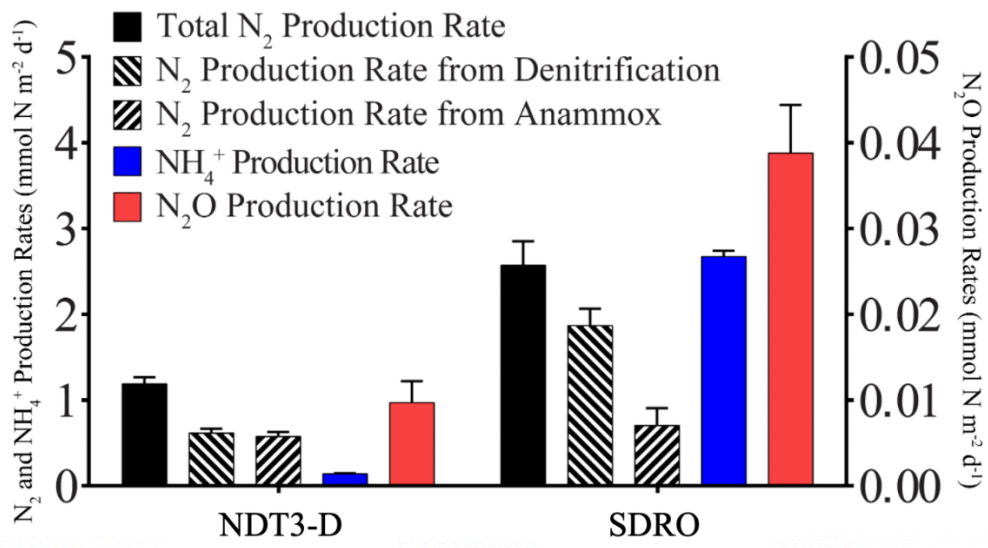
498
499
500 **Figure 6.** Areal rates of total N_2 production, denitrification, anammox, NH_4^+ production (DNRA), and N_2O
501 production
502

503

4. Discussion

4.1 Giant sulfur-oxidizing bacterial mats proliferated in response to deoxygenation in the Santa Barbara Basin

The SBB is an ideal environment to study the effect of transient deoxygenation on benthic biogeochemistry. In Fall 2019, when this expedition took place, the SBB was undergoing a transition from oxygenated to virtually anoxic conditions (Qin et al., 2022). When the AT42-19 cruise occurred, most of the bottom water in the basin was hypoxic (A-, B-, C-, and D-stations), except for the depositional center. Separate O_2 measurements from the ROV sensor (O_2 below detection limit, Table 1), microprofilers (no signal change between water column and sediment, Fig. 4), and Winkler titration from CTD/rosette casts (uniform non-zero value below 500 m (Qin et al., 2022)) indicated full anoxia in the bottom water at the deeper stations (NDRO and SDRO). Notably, bottom water conditions revealed a slight asymmetry between the basin transects (Fig. 1); bottom water along the northern transect generally had more O_2 and NO_3^- than the southern transect (e.g., 9 μM O_2 at NDT3-A and 0 μM O_2 at SDT3-A). This asymmetry indicated differences in the circulation and/or microbial communities between the northern and southern portions of the basin. Whether this asymmetry is a permanent feature of the basin or symptomatic of the specific conditions in November 2019 is unclear; previous studies in the SBB have been restricted to the depocenter or one side of the basin (Sholkovitz, 1973; Reimers et al., 1996; Kuwabara et al., 1999). Regardless of bottom water oxidant concentration, the energetically most favorable terminal electron acceptors (O_2 and NO_3^-) disappeared in a very narrow zone below the sediment-water interface (Fig. 4 and Figs. 2 and 3, respectively), consistent with their expected rapid consumption by the benthic microbial community.

527   In the present study, benthic GSOB mats were primarily limited to the anoxic depocenter of the

528   SBB. Similarly, such mats were replete in the core of the anoxic Peruvian OMZ (Levin et al.,

529   2002; Sommer et al., 2016; Mosch et al., 2012), but absent from the seafloor below the hypoxic,

530   i.e., slightly oxygenated, Mauritanian OMZ (Schroller-Lomnitz et al., 2019). GSOB mats in

531   November 2019 were observed deeper in the basin than in October 2013 (Valentine et al., 2016)

532   but in a similar location to June 1988 (Reimers et al., 1996) and April 1997 (Kuwabara et al.,

533   1999). During the 2013 sampling, dense GSOB mats were confined to depths between approx.

534   500-570 m (equivalent to the B-stations from this expedition), corresponding with anoxic

535   conditions in the bottom water. This habitat was sandwiched between an anoxic, anitric (i.e.,

536   nitrate-free) deep and a hypoxic, nitrigenated (i.e., nitrate-rich) shallower water layer (Valentine

537   et al., 2016). The difference in depth distribution of GSOB mats between the 2013 and 2019

538   expedition provides evidence that GSOB mats in the SBB are ephemeral and proliferate where

539   the bottom water is anoxic but not anitric.

540

541   As our study represents only a snapshot of an oxygen- and nitrate-driven mat dynamic, we can

542   only speculate how areas of the basin that did not contain GSOB mats in November 2019 fit into

543   this dynamic. For example, mat-forming sulfur bacteria found slightly deeper in the sediment at

544   B-stations (see section 3.2) could be progenitors to surface sediment colonization of thick GSOB

545   mats, as has been recorded in other transiently deoxygenated environments (Jørgensen, 1977).

546   Alternatively, these subsurface colonies could also be remnants of a former surface GSOB mat

547   that retreated under changing redox conditions. Oxygenated conditions in the water preceding

548   the 2019 expedition would, in this context, suggest the mats migrated following a previous

549   anoxic event (Qin et al., 2022). If deoxygenation persisted in the SBB after the AT42-19 cruise,

550   then anitria (i.e., anitric conditions – similar to anoxia) would likely follow in the deepest basin

551   water. These conditions would be similar to those seen in 2013 (Valentine et al., 2016), where

552   GSOB mats formed a contiguous "donut ring" at shallower basin depths. Interestingly, GSOB

553   mats in the Eastern Gotland Basin of the Baltic Sea were confined to a hypoxic transition zone,

554   where O_2 was < 30 µM but did not reach anoxia, while no mats were observed at deeper anoxic

555   locations (Noffke et al., 2016). This difference in distribution compared to the SBB suggests that

556   GSOB mats proliferate under different conditions (anoxic or hypoxic), potentially depending on

557   the species of mat-forming bacteria present and whether they specialize in aerobic or anaerobic

558   chemosynthesis.

559

560   **4.2 Shift from benthic denitrification to dissimilatory nitrate reduction to ammonium in**

561   **response to complete deoxygenation in the Santa Barbara Basin**

562

563   Benthic uptake and release of nitrogen species by SBB sediment appeared to be affected by the

564   presence of GSOB mats. While total benthic nitrate uptake was similar between D- and

565   depocenter stations based on in-situ NO_3^- flux measurements (Fig. 4), NH_4^+ release from the

566   sediment into the water column increased where GSOB mats were present (Fig. 5). This trend is

567   supported by the porewater profiles of NH_4^+, which showed a steeper increase over sediment

568   depth at deeper stations (Figs. 2 & 3). Incubations with ^{15}N-NO_3^- revealed that N_2 production

569   (denitrification and anammox) accounted for 86% of NO_3^-/NO_2^- reduction in the shallow basin,

570   while NH_4^+ production (DNRA) accounted for 13% and N_2O production accounted for 1%

571   (NDT3-D, Fig. 6;(Peng et al., 2023)). In contrast, most (54%) of NO_3^- reduction at the

572   depositional center occurred via DNRA; N_2 production accounted for 45% and N_2O production

573 accounted for 1% of NO_3^- reduction at the SDRO (Fig. 6; Peng et al. 2023). It is important to

574 note that these results only describe patterns of NO_3^- reduction in the basin, while other

575 mechanisms of nitrate uptake by sediment (e.g., hyper-accumulation of nitrate into vacuoles) are

576 more difficult to calculate accurately.

577

578 It is likely important to SBB benthic nitrogen cycling that some eukaryotic organisms can hyper-

579 accumulate NO_3^- in benthic, anoxic environments including diatoms (Kamp et al., 2011) and

580 foraminifera (Risgaard-Petersen et al., 2006). Additionally, meiofauna (e.g., nematodes) can

581 enhance rates of denitrification (Bonaglia et al., 2014). Both foraminifera and meiofauna were

582 observed in SBB depocenter and A-station sediments in November 2019, and diatoms were

583 observed in shallower sediments in the basin (data not shown). Other studies found that benthic

584 foraminifera in the SBB depocenter can hyperaccumulate NO_3^- intracellularly up to 375 ± 174

585 mM (Bernhard et al., 2012) and host symbionts capable of performing denitrification (Bernhard

586 et al., 2000). These foraminifera were found to be responsible for approx. 3 mM N m^{-2} d^{-1}, or

587 67% of the total denitrification occurring in the SBB depocenter (Bernhard et al., 2012).

588 Additionally, fungi could reduce NO_3^- or NO_2^- to nitrous oxide in marine sediments and may

589 contribute to denitrification in SBB sediments (Kamp et al., 2015; Lazo-Murphy et al., 2022).

590 This opens up the possibility that the majority of denitrification we observed in the SBB

591 depocenter is performed by eukaryotes, while prokaryotes (especially GSOB) are responsible for

592 most of the DNRA. Elevated NO_3^- and NO_2^- concentrations that were observed in our 0-1 cm

593 samples from NDT3-A and SDRO have been reported from SBB depocenter sediments in the

594 past (Reimers et al., 1996; Bernhard et al., 2003), and have been attributed to both GSOB and benthic

595 eukaryotes. The impact of eukaryotes on SBB benthic nitrogen transformation remains to be disentangled

596 from the mats themselves.

597

598

599 Our data suggests a transition from denitrification-dominated sediment in the oxygenated basin

600 to an increasing influence of DNRA on N cycling in the deeper, anoxic basin. Placed in the

601 context of other OMZs, Mauritanian shelf sediment was dominated by denitrification (Dale et al.,

602 2014), similar to SBB shallow sediment (below hypoxic water) while core Peruvian OMZ

603 sediment was dominated by DNRA, similar to sediment of the deeper SBB (below anoxic water)

604 (Sommer et al., 2016). Nitrate reduction in sediment below the seasonally hypoxic Eckernförde

605 Bay (Dale et al., 2011) and below the hypoxic transition zone of the Eastern Gotland Basin

606 (Noffke et al., 2016) also showed increased DNRA where GSOB mats were present, though with

607 an order of magnitude lower NH_4^+ flux (avg. 1.74 mmol m^{-2} d^{-1} and max. 1.10 mmol m^{-2} d^{-1},

608 respectively) than the SBB depocenter.

609

610 While our study suggests a shift from denitrification to DNRA during deoxygenation of SBB

611 bottom water, other studies examined changes in benthic nitrogen cycling under reverse

612 conditions, i.e., the reoxidation of the environment following anoxia (Hylén et al., 2022; De

613 Brabandere et al., 2015). After a decadal oxygenation event in the Eastern Gotland Basin (Baltic

614 Sea) in 2015-2016, sediment exhibited a slight increase in denitrification, but remained

615 dominated by DNRA and N_2O production (Hylén et al., 2022). The lack of N_2 production via

616 denitrification following this oxygenation event was attributed to the reoxygenation event being

617 too weak to substantially oxidize sediments, which would favor denitrification (Hylén et al.,

618 2022). In an engineered reoxygenation event of the By Fjord on Sweden's western coast, where

619 dissolved O_2 and NO_3^- content of anoxic and anitric bottom water was artificially increased to

620   approx. 130 µM O_2 and 20 µM NO_3^- over a period of roughly 2 years, denitrification rates were

621   increased by an order of magnitude and DNRA rates were also stimulated (De Brabandere et al.,

622   2015). Comparing our results to these two studies suggests that DNRA bacteria are more

623   resilient to weak reoxygenation events and thrive in transiently deoxygenated systems that

624   remain hypoxic ($O_2 < 63$ µM). The frequency and magnitude of reoxygenation and

625   deoxygenation of SBB bottom waters, and the effect of these processes on the benthic microbial

626   community, could be a major factor supporting some of the highest recorded total nitrate

627   reduction rates in a natural benthic marine setting (Peng et al., 2023).

628
629
630 **Table 3.** Example reactions of nitrate reduction pathways with associated energy yield in respect to the electron donor (H_2 or HS^-) and electron acceptor (NO_3^-) and electron accepting capacity. Modified from Table 2 in (Tiedje et al., 1983).

Reaction	$\Delta G^{\circ\prime}$ (kcal mol^{-1})		Electrons per NO_3^-
	H_2 / HS^-	NO_3^-	
Chemoheterotrophic Denitrification			
$2NO_3^- + 5H_2 + 2H^+ \rightarrow N_2 + 6H_2O$	-53.6	-133.9	5
Chemoautotrophic Denitrification			
$8NO_3^- + 5HS^- + 3H^+ \rightarrow 5SO_4^{2-} + 4N_2 + 4H_2O$	-177.9	-111.2	5
Chemoheterotrophic DNRA			
$NO_3^- + 4H_2 + 2H^+ \rightarrow NH_4^+ + 3H_2O$	-35.8	-143.3	8
Chemoautotrophic DNRA			
$NO_3^- + HS^- + H^+ + H_2O \rightarrow NH_4^+ + SO_4^{2-}$	-107.0	-107.0	8

631

632

633   A high ratio of electron donor to electron acceptor favors DNRA over denitrification (Marchant

634   et al., 2014; Hardison et al., 2015; Tiedje et al., 1983) and this ratio appears to be critical in

635   determining the dominant nitrate reduction pathway in SBB sediments, similar to the Eastern

636   Gotland Basin (Hylén et al., 2022) and the By Fjord (De Brabandere et al., 2015). Example

637   energy yields for denitrification and DNRA are shown in Table 3. As discussed in (Tiedje et al.,

638   1983), heterotrophic denitrification yields more energy per mol of electron donor than DNRA.

639   However, the reverse is true when considering energy yield per mol of electron acceptor (NO_3^-).

640   DNRA also yields 3 more electrons per molecule of NO_3^- than denitrification. Tiedje et al.

641   argued that in environments that are starved of powerful terminal electron acceptors, such as

642   anoxic, organic-rich sediment, the energy yield per electron acceptor and additional electrons

643   available for transfer could push nitrate reduction towards DNRA. Multiple laboratory and

644   model studies have converged on an electron donor to acceptor ratio of approximately 3 to

645   encourage DNRA over denitrification (Hardison et al., 2015; Algar and Vallino, 2014) though

646   other studies have found higher values (Porubsky et al., 2009; Kraft et al., 2014). Sulfide

647   concentrations near the sediment-water interface at the SBB depocenter (approx. 200 µM at 0.5

648   cm depth; Fig. 3, NDRO) would favor chemoautotrophic DNRA over denitrification at ambient

649   marine nitrate concentrations (approx. 28 µM). Additionally, DNRA appears to be the preferred

650   nitrate reduction pathway for chemoautotrophs that utilize iron or sulfide as an electron donor

651   (Caffrey et al., 2019; Kessler et al., 2019; An and Gardner, 2002). As GSOB mats hyper-

652   accumulate nitrate from the bottom water into their intracellular vacuoles, the resulting decline in

653   electron acceptors at the sediment-water interface coupled with an elevation of the sulfate

654   reduction zone would create an electron donor to acceptor ratio that favors DNRA. Since GSOB

655   mats in the SBB seem to prefer DNRA, starving the bottom water of electron acceptors coupled

656   with the high sulfate reduction rates could give them a competitive advantage and allow them to

657   proliferate into the largest-yet mapped GSOB mat in Earth's oceans, as seen in other expeditions

658   (Valentine et al., 2016; Reimers et al., 1996; Kuwabara et al., 1999).

659

660   **4.3 Microbial mat proliferation and benthic phosphate remineralization dependent on high**

661   **rates of organic matter degradation in the Santa Barbara Basin**

662

663 Organic carbon content of the benthic environment appears to be a key control on sulfate

664 reduction rates near the sediment-water interface as well as microbial mat proliferation. Sulfate

665 reduction rates in the SBB depocenter are most similar in magnitude and profile (i.e., highest

666 rates found at the sediment-water interface and decline drastically thereafter) to those found in

667 sediments below the transiently deoxygenated portion of the Peruvian shelf (e.g., 4.1 mmol m^{-2}

668 d^{-1} at the SBB NDRO station vs. 2.5-3.8 mmol m^{-2} d^{-1} at 128-144 m water depth on the Peruvian

669 margin (Gier et al., 2016; Treude et al., 2021)). The TOC content of surface sediments in these

670 two regions are both high and within the same order of magnitude (maximum recorded TOC of

671 5.2% at the 0-1 cm margin at the SDT1-A station compared with 7.6% in the Peruvian margin

672 145 m depth (Noffke et al., 2012)). In comparison, sulfate reduction rates in the SBB were at

673 least one order of magnitude lower than found in sediment below the OMZ on the Namibian

674 Shelf, which has much higher TOC contents of >10% (Brüchert et al., 2003; Bremner, 1981).

675 Sulfate reduction rates in the shelf sediments below the Eastern Arabian OMZ were much lower

676 (0.18 – 1.27 mmol m^{-2} d^{-1}) than rates in the SBB depocenter (Naik et al., 2017) despite similar

677 hypoxic to anoxic bottom water conditions. These lower sulfate reduction rates were attributed to

678 the relatively low amount of pelagic primary productivity and ergo benthic organic matter

679 delivery in the Eastern Arabian OMZ compared to other upwelling systems (Naik et al., 2017).

680 The organic matter content of the sediment appears to be important in the proliferation of GSOB

681 mats; too much TOC could result in toxic levels of sulfide at the sediment-water interface

682 (*Beggiatoa* exhibit an aversion to sulfidic sediments but toxicity has not been quantified)

683 (Preisler et al., 2007), whereas too little sulfide would not provide enough electron donor for the

684 GSOB's chemoautotrophic metabolism.

685

686   The profiles of several indicators for benthic anaerobic organic matter remineralization (total

687   alkalinity, DIC, PO_4^{3-}, NH_4^+) increased in steepness with increasing water depth (Figs. 2 A-E &

688   3A-F). One divergence from this trend can be seen in PO_4^{3-} profiles from the shallow C- and D-

689   stations, which also featured low rates of sulfate reduction. PO_4^{3-} profiles in these sediments

690   track closely to Fe^{2+} profiles; both solutes dip in concentration in areas with visible iron sulfide

691   formation (e.g., 5-11 cm in NDT3-D as seen in Fig. 2A). Additionally, several stations that

692   exhibited high sulfate reduction rates in surface sediment (e.g., SDT1-A) showed almost no

693   change in PO_4^{3-} at depths below 5 cm (e.g., Fig. 2 K-O compared to Fig. 2 A-E). This

694   phenomenon has been previously documented in SBB sediment and is attributed to the

695   precipitation of carbonate fluorapatite (Reimers et al., 1996). The confinement of these flat PO_4^{3-}

696   profiles to stations with >100 nmol cm^{-3} d^{-1} sulfate reduction in surface sediment suggests that

697   this mineralogical sink of PO_4^{3-} in SBB sediment may be dependent on high sulfate reduction

698   rates, owing to the bicarbonate produced by sulfate reduction (Reimers et al., 1996), and is not

699   found throughout the basin. Flat PO_4^{3-} profiles were also reported from the transiently

700   deoxygenated portion of the Peruvian OMZ, where phosphate mineral precipitation has been

701   documented (Noffke et al., 2012). Similar to the shallow margins of the SBB, PO_4^{3-} in

702   Mauritanian OMZ porewater tracks closely with changes in porewater Fe^{2+} (Schroller-Lomnitz

703   et al., 2019), indicating that iron mineralization/dissolution mechanisms hold a greater influence

704   on PO_4^{3-} concentrations under hypoxic bottom waters.

705

706   **4.4 Iron oxide exhaustion is critical for raising the sulfate reduction zone close to the**

707   **sediment-water interface in Santa Barbara Basin sediment.**

708

709   The hyper-accumulation of NO_3^- by GSOB mats potentially facilitates sulfate reduction close to

710   the sediment-water interface in the SBB (e.g., NDRO and NDT3-A as seen in fig. 2N and 2O) by

711   starving the sediment of this more powerful electron acceptor. The rise of the sulfate reduction

712   zone at NDT3-C (fig. 2L) further suggests that the exhaustion of iron oxides and the formation of

713   iron sulfide below the sediment-water interface may play a crucial role in controlling the

714   distribution of sulfate reduction as well. SBB sediments showed a wide vertical and horizontal

715   heterogeneity of redox states based on visual appearance (Fig. 1A-K). Sediment beneath the

716   hypoxic bottom water at the shallowest D-stations was reddish, consistent with a high content of

717   iron oxides. Interestingly, porewater Fe^{2+} concentrations in shallower parts of the basin (e.g.,

718   NDT3-D, max. ~700 µM Fe^{2+}) were an order of magnitude larger than those found in both the

719   Peruvian (max ~60 and ~30 µM Fe^{2+}, respectively; (Noffke et al., 2012; Plass et al., 2020) and

720   Mauritanian (max. ~50 µM Fe^{2+}; Schroller-Lomnitz et al 2019) OMZ. It should be noted that

721   porewater samples for geochemical analyses were unfiltered and hence reported iron

722   concentrations include aqueous, colloidal, and nanoparticulate species. Regardless, all these

723   components represent bioavailable sources of iron. Further, since filtering through 0.45 or 0.2

724   µm filters only removes a fraction of colloidal particles and no nanoparticles (Raiswell and

725   Canfield, 2012), potential surplus porewater iron in SBB samples in comparison to studies that

726   applied filtering was likely minimal.

727

728   Deeper in the basin, bands of black sediment that appear mid-core at NDT3-C (6-14 cm) and

729   SDT3-C (6-10 cm) indicate the formation of iron sulfides as a result of sulfide produced by

730   sulfate reduction (Canfield, 1989). Both D-stations had similar bottom water conditions (Table

731   1), sulfate reduction rates (Fig. 3W-AG), porewater concentrations of solutes (Figs. 2 and 3), and

732   visual sediment characteristics (Section 3.1). On the contrary, there are some noticeable

733   differences in the porewater geochemistry between the two C-stations. At the C-stations, peaks

734   in sulfate reduction were in the surface sediment, above the iron sulfide layers, and declined

735   below approximately 4 cm, indicating a discrepancy between observed peak sulfate reduction

736   activity and the mineralogical clues left behind by the process. Comparing NDT3-C and SDT3-

737   C, iron sulfide formation (Table 1B compared to 1J), porewater Fe^{2+} profiles (Fig. 2G compared

738   to Fig. 3H), and sulfate reduction rates (Fig. 2L compared to Fig. 3N) show that NDT3-C

739   sediment appears to be in transition towards a more sulfidic state, while SDT3-C sediments still

740   mimic the shallow D-station ferruginous state. While sulfate reduction rates for B-stations are

741   not available due to technical issues during sample processing, porewater Fe^{2+} profiles show a

742   similar difference between the north and south basin (Fig. 2H compared to Fig. 3I) as did visual

743   sediment characteristics (Table 1C compared to 1I). This difference in biogeochemical profiles

744   and apparent minerology between the north and south C- and B-stations could be a result of

745   hydrographic and/or bathymetric differences in the basin (Sholkovitz and Gieskes, 1971; Bograd

746   et al., 2002), but a discernable link between the differences in sediment biogeochemistry and the

747   differences in bottom water oxygen (Table 1) need to be further explored.

748

749   Deeper in the basin (depocenter and A-stations), porewater Fe^{2+} concentrations in sediment

750   beneath anoxic bottom water (max. 84 µM Fe^{2+}) were similar to concentrations found below the

751   Peruvian OMZ in 2008 under anoxic bottom water conditions (78 m water depth, max. 80 µM

752   Fe^{2+}) (Noffke et al., 2012). These deep basin porewater Fe^{2+} concentrations were, however, an

753   order of magnitude larger than those found at a similar site on the Peruvian shelf (75 m water

754   depth, max. 1 µM Fe^{2+}) in 2017 during a kelvin-wave-associated "Coastal El Niño" event that

755   created oxygenated bottom waters during the sampling and the disappearance of previously

756   observed dense GSOB mats (Plass et al., 2020). As the SBB water column was undergoing rapid

757   deoxygenation in the weeks preceding this study (Qin et al., 2022), the sediments below the sill

758   appeared to be actively shifting from a ferruginous state to a sulfidic state, with this change

759   starting around the C-stations and being complete in the depocenter. Comparing apparent iron

760   sulfide formation with dips in porewater Fe^{2+} concentrations in C-station profiles (Fig. 1B

761   compared to Fig. 2G and Fig. 1J compared to Fig. 3H) signals a shift away from a ferruginous

762   state occurring just below the SBB sill.

763

764   C-station porewater Fe^{2+} concentrations and sulfate reduction rates indicate that migration of the

765   sulfate reduction zone towards the sediment-water interface is associated with iron sulfide

766   formation deeper in the sediment. The activity (or lack thereof) of cable bacteria, which are able

767   to bridge the gap between the oxidized sediment-water interface and reduced sediment below

768   using a biofilament (Pfeffer et al., 2012), could explain the interplay between sulfate reduction

769   and iron cycling in SBB sediments. Cable bacteria, such as *Ca. Electronema* sp., contain genes

770   involved in DNRA (Kjeldsen et al., 2019) and can perform nitrate reduction in incubation

771   experiments (Marzocchi et al., 2014), but their direct transformation of NO_3^- in the environment

772   appears limited (Kessler et al., 2019) and they appear to be inactive in anoxic aquatic

773   environments (Seitaj et al., 2015; Marzocchi et al., 2018; Hermans et al., 2019). Cable bacteria

774   primarily conduct aerobic sulfide oxidation (Pfeffer et al., 2012), though they can also utilize

775   Fe^{2+} as an electron donor (Seitaj et al., 2015). The maximum recorded filament length of cable

776   bacteria is 7 cm (Van De Velde et al., 2016), though typically they are not stretched completely

777   vertically through the sediment. The appearance of black sediment in the SBB C-station

778   sediments, starting at approx. 5 cm depth, could be an indication that cable bacteria are oxidizing

779   iron sulfides at that sediment depth and prevent their formation at shallower depths. Further,

780   cable bacteria have been found to directly compete with GSOB in transiently deoxygenated

781   systems, with cable bacteria active under oxygenated conditions and GSOB active in anoxic

782   conditions (Seitaj et al., 2015). Cable bacteria can also prevent the benthic release of sulfide,

783   which is toxic to many pelagic animals, via the creation of an iron-oxide buffer (formed through

784   Fe^{2+} oxidation) in near-surface sediments (Seitaj et al., 2015). Therefore, if cable bacteria activity

785   in the SBB decreased with declining oxygen concentrations below the sill, the iron oxide buffer

786   they create could have been reduced, encouraging the sulfate reduction zone to migrate towards

787   the sediment surface (as seen at NDT3-C). Cable bacteria can sometimes be detected in

788   sediments via a slight pH increase (typically pH > 8) (Schauer et al., 2014) which was not

789   reflected in our pH results, but this phenomenon is more typically seen in the laboratory and not

790   the field (Hermans et al., 2019).

791

792   **4.5 Iron and phosphate flux into SBB bottom water is a feature of transient deoxygenation.**

793

794   Release of dissolved iron and phosphate from sediment below anoxic waters is a well-

795   documented phenomenon (e.g., (Mortimer, 1941; Van Cappellen and Ingall, 1994; Van De

796   Velde et al., 2020; Noffke et al., 2012)) and this phenomenon is seen in the SBB as well. As

797   postulated previously (Kuwabara et al., 1999), basin flushing oxidizes iron sulfides at the

798   sediment-water interface, providing ample substrate for microbial iron reduction once anoxia

799   returns. This iron reduction initiates high rates of Fe^{2+} release from SBB depocenter sediment

800   (Fig. 5). Iron reduction further releases iron-bound PO_4^{3-} (Mortimer, 1941) as seen by high

801   benthic fluxes of PO_4^{3-} at the depocenter (Fig. 5), although notably some of this PO_4^{3-} release is

802   likely attributed to organic matter degradation (Van Cappellen and Ingall, 1994). High benthic

803   Fe^{2+} and PO_4^{3-} fluxes were also seen on the Peruvian shelf during transient anoxia (Noffke et al.,

804   2012). The release of these solutes was interpreted to be sourced from a layer of reactive iron

805   hydroxides existing near the sediment surface, likely established during a recent oxygenation

806   event. Similar conditions, i.e., visibly oxidized (reddish) sediment laminae and a thin zone of

807   iron reduction apparent from a peak in Fe^{2+} at the sediment-water interface, were found in

808   sediment from the SBB depocenter. Deeper in the persistently anoxic core of the Peruvian OMZ,

809   sediment appears to have little to no flux of Fe^{2+} and PO_4^{3-} into the bottom water (Noffke et al.,

810   2012). Here, iron at the sediment-water interface is hypothesized to be locked up in iron sulfides,

811   which are rarely re-oxidized due to persistent anoxia.

812

813   In a different study from the Eastern Gotland Basin in the Baltic Sea, enhanced elemental fluxes

814   were observed during a decadal oxygen flushing event (Van De Velde et al., 2020), which was

815   attributed to enhanced elemental recycling, or cycles of mineral precipitation in the water column

816   followed by mineral dissolution once those minerals sink to the sediment. Notably, the iron flux

817   observed in the Eastern Gotland Basin (max. 0.08 mmol m^{-2} d^{-1}) (Van De Velde et al., 2020) was

818   two orders of magnitude lower than the flux observed in the anoxic depocenter of the Santa

819   Barbara Basin (max. 4.9 mmol m^{-2} d^{-1}). It is further notable that benthic fluxes of PO_4^{3-} in the

820   SBB depocenter were also an order of magnitude higher than fluxes in the Eastern Gotland

821   Basin's hypoxic transition zone (3.6 vs. 0.23 mmol PO_4^{3-} m^{-2} d^{-1}) - both of which contained

822   GSOB mats, but while the SBB was anoxic and the Eastern Gotland Basin was hypoxic (Noffke

823   et al., 2016). These differences in Fe^{2+} and PO_4^{3-} flux between the SBB and the Eastern Gotland

824   Basin suggest that reoxidation of the sediment-water interface during basin flushing, as opposed

825   to water-column-associated reoxidation, appears to encourage higher benthic iron fluxes.

826

827   Fe^{2+} and PO_4^{3-} flux from the SBB depocenter were also approximately five times higher (Fig. 5)

828   compared to the anoxic Peruvian shelf (4.9 vs. 0.9 mmol Fe^{2+} m^{-2} d^{-1} and 3.6 vs. 0.8 mmol PO_4^{3-}

829   m^{-2} d^{-1}, respectively) (Noffke et al., 2012). Based on Fe^{2+} profiles, the zone of iron reduction in

830   Peruvian shelf sediments extended down to approx. 10 cm, while the zone appeared to be much

831   shallower and narrower (less than the top 5 cm) in the SBB depocenter. These differences in

832   magnitude of Fe^{2+} concentration and Fe^{2+} and PO_4^{3-} flux between the SBB depocenter and the

833   Peruvian shelf could be attributed to differences in the recency and magnitude of reoxygenation

834   events. The release of Fe^{2+} from sediment into the bottom water could create a buffer against

835   reoxygenation in transiently deoxygenated systems, giving a competitive advantage to anaerobic

836   benthic metabolisms (Dale et al., 2013; Wallmann et al., 2022). Additionally, both Fe^{2+} and

837   PO_4^{3-} release from the SBB sediment could allow for higher rates of primary productivity if

838   those constituents diffused into the photic zone (Robinson et al., 2022). The fate of Fe^{2+} and

839   PO_4^{3-} diffusing into SBB waters from the sediment-water interface is a focus of ongoing work

840   within the basin.

841
842   **5 Conclusions**
843

844   This research expands upon the wealth of science already conducted in the SBB and other

845   transiently deoxygenated environments by examining changes in benthic biogeochemistry

846   promoted by the onset of anoxia. Our main interpretations are summarized in Fig. 7. We found

847   that GSOB mats proliferate in the SBB where the bottom water is anoxic and nitrate

848   concentrations are declining (Fig. 7, A- and depocenter stations). Nitrate uptake by SBB

849   sediment is similar regardless of GSOB mat presence, but these mats appear to initiate a shift

850   from denitrification to DNRA as the primary nitrate reduction pathway (Fig. 7, beginning at B-

851   stations). The zone of sulfate reduction rises to the sediment-water interface where GSOB mats

852   are present (Fig. 7, A-stations), possibly because the hyper-accumulation of nitrate into their

853   intracellular vacuoles starves the environment of this more powerful electron acceptor. However,

854   following the natural order of electron acceptor utilization (Boudreau and Jorgensen, 2001), iron

855   oxides near the sediment-water interface must be exhausted before sulfate reduction can

856   dominate surface sediments and GSOB mats can proliferate in the SBB (Fig. 7, depocenter

857   stations). If anoxic events become longer and more frequent in the SBB because of global

858   warming (see, e.g., (Qin et al., 2022; Stramma et al., 2008)), the iron oxide buffer built up in

859   shallower basin depths could be exhausted, allowing for surface sulfate reduction and the

860   proliferation of GSOB mats in shallower margins of the basin than currently seen. Further, the

861   same transient deoxygenation that allows for these mats to re-stablish themselves also allows for

862   a high Fe^{2+} and PO_4^{3-} flux into the SBB water column. In order to fully understand the complex

863   changes in the benthic environment in response to deoxygenation, genomic and molecular work

864   of the upper sediment community needs to be characterized. Overall, the insights gleaned from

865   this research will aid in the understanding of fundamental biogeochemical changes that occur

866   when marine environments become anoxic.

867
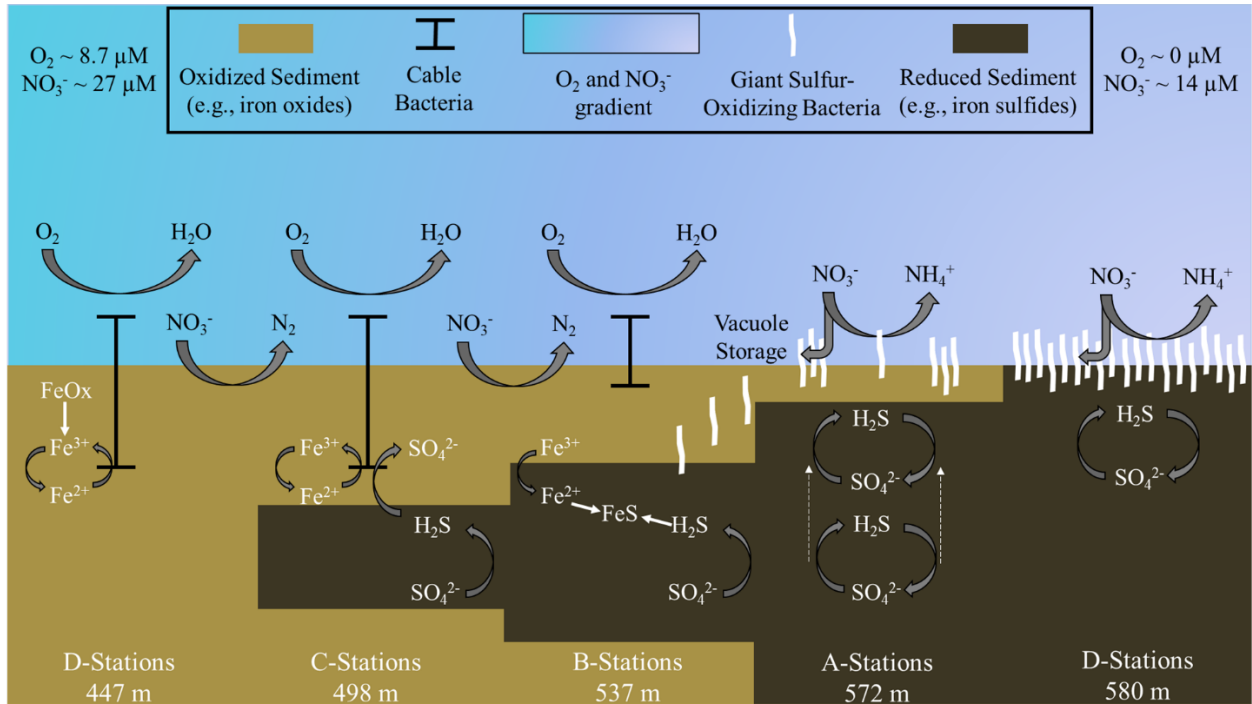
Figure 7: Schematic of biogeochemical processes in the Santa Barbara Basin along the depth gradients studied in October/November 2019. Teal to lavender gradient represents a decline in O_2 and NO_3^- concentrations with basin depth. In the shallower, hypoxic basin (D-stations), denitrification and iron reduction are dominant and reduced iron is rapidly re-oxidized in near-surface sediment by cable bacteria. Deeper in the basin (A-stations and depocenter), nitrogen cycling shifts towards dissimilatory nitrate reduction to ammonia (DNRA). Reduced iron combines with sulfide, produced by sulfate reduction, diffusing from deeper sediment layers to form iron sulfides. As oxygen concentration approaches zero between the A-stations and the basin's depocenter, giant sulfur-oxidizing bacteria hyper-accumulate nitrate in their intracellular vacuoles. Nitrate removal combined with the exhaustion of available iron oxides in the near-surface sediments allows the zone of sulfate reduction to migrate towards the surface (see dashed arrows at A-stations), providing the giant sulfur-oxidizing bacteria with sufficient reduced sulfur to proliferate into thick, contiguous mats. Note: Figure is not to scale, and processes are simplified to illustrate main concepts.

Acknowledgements

881

882   We thank the captain, crew, and scientific party of the R/V Atlantis, and the crew of the ROV

883   Jason for their technical and logistical support during the research expedition AT42-19. We also

884   thank Q. Qin, E. Arrington, M. O'Beirne, A. Mazariegos, X. Moreno, A. Eastman, and K.

885   Gosselin for assisting with shipboard analyses. We thank J. Liu for assistance in reviewing the

886   data processing for this manuscript. We further thank M. Alisch from the Max-Planck-Institute

887   in Bremen, Germany for DIC analyses. We thank G. Eickert-Grötzschel, V. Hübner, A. Niclas, I.

888   Schröder, and C. Wigand from the Max-Planck-Institute in Bremen, Germany for constructing

889   the microsensors. We acknowledge J. Matthews from the UC Davis Stable Isotope facility for

890   assisting with solid phase analyses. Funding for this work was provided by the US National

891   Science Foundation, NSF OCE-1756947 and OCE-1830033 (to DLV) and OCE-1829981 (to

892   TT), and a Simons Foundation Postdoctoral Fellowship in Marine Microbial Ecology (No.

893   547606 to XP). Further support was provided by the Max Planck Society and the Alfred

894   Wegener Institute for Polar and Marine Research.

895

896   **Data availability.**

897   Biogeochemical data presented in this manuscript are accessible through the Biological &

898   Chemical Oceanography Data Management Office (BCO-DMO) at the following landing pages:

899   https://www.bco-dmo.org/dataset/867007; https://www.bco-dmo.org/dataset/867113;

900   https://www.bco-dmo.org/dataset/867221; https://www.bco-dmo.org/dataset/896706

901 **Author contributions.**

902 TT, DV, FK, NL, and JT designed the project. DJY, SK, JT, DR, and TT processed sediment

903 cores at sea. DJY conducted geochemical analyses of sediment porewater and benthic flux

904 chamber water. DJY prepared TOC and TON samples. DR and SK analyzed sediment porosity

905 and density. TT and SK performed shipboard sulfate reduction incubations. DJY and DR

906 conducted sulfate reduction analyses. DJY, NL, and JT transformed and interpreted ROV Jason

907 data. FJ and FW operated BFC and microprofilers and analyzed associated data. XP conducted

908 ^{15}N experiments and analyses. All authors reviewed and edited the manuscript.

909

910 **Competing interests.**

911 At least one of the (co-)authors is a member of the editorial board of Biogeosciences.

References

912 **References**
913
914 Algar, C. K. and Vallino, J. J.: Predicting microbial nitrate reduction pathways in coastal
915   sediments, Aquatic Microbial Ecology, 71, 223-238, 2014.
916 An, S. and Gardner, W. S.: Dissimilatory nitrate reduction to ammonium (DNRA) as a nitrogen
917   link, versus denitrification as a sink in a shallow estuary (Laguna Madre/Baffin Bay,
918   Texas), Marine Ecology Progress Series, 237, 41-50, 2002.
919 Bernhard, J. M., Visscher, P. T., and Bowser, S. S.: Submillimeter life positions of bacteria,
920   protists, and metazoans in laminated sediments of the Santa Barbara Basin, Limnology
921   and Oceanography, 48, 813-828, 2003.
922 Bernhard, J. M., Buck, K. R., Farmer, M. A., and Bowser, S. S.: The Santa Barbara Basin is a
923   symbiosis oasis, Nature, 403, 77-80, 2000.
924 Bernhard, J. M., Casciotti, K. L., McIlvin, M. R., Beaudoin, D. J., Visscher, P. T., and Edgcomb, V.
925   P.: Potential importance of physiologically diverse benthic foraminifera in sedimentary
926   nitrate storage and respiration, Journal of Geophysical Research: Biogeosciences, 117,
927   2012.
928 Bograd, S. J., Schwing, F. B., Castro, C. G., and Timothy, D. A.: Bottom water renewal in the
929   Santa Barbara Basin, Journal of Geophysical Research: Oceans, 107, 9-1-9-9, 2002.
930 Bonaglia, S., Nascimento, F. A., Bartoli, M., Klawonn, I., and Brüchert, V.: Meiofauna increases
931   bacterial denitrification in marine sediments, Nature communications, 5, 5133, 2014.
932 Boudreau, B. P. and Jorgensen, B. B.: The benthic boundary layer: Transport processes and
933   biogeochemistry, 2001.
934 Bourbonnais, A., Letscher, R. T., Bange, H. W., Echevin, V., Larkum, J., Mohn, J., Yoshida, N.,
935   and Altabet, M. A.: N2O production and consumption from stable isotopic and
936   concentration data in the Peruvian coastal upwelling system, Global Biogeochemical
937   Cycles, 31, 678-698, 2017.
938 Bremner, J.: Biogenic sediments on the South West African continental margin, 1981.
939 Brüchert, V., Jørgensen, B. B., Neumann, K., Riechmann, D., Schlösser, M., and Schulz, H.:
940   Regulation of bacterial sulfate reduction and hydrogen sulfide fluxes in the central
941   Namibian coastal upwelling zone, Geochim. Cosmochim. Acta, 67, 4505-4518, 2003.
942 Caffrey, J. M., Bonaglia, S., and Conley, D. J.: Short exposure to oxygen and sulfide alter
943   nitrification, denitrification, and DNRA activity in seasonally hypoxic estuarine
944   sediments, FEMS microbiology letters, 366, fny288, 2019.
945 California Cooperative Oceanic Fisheries Investigations: https://www.calcofi.org/ccdata.html,
946   last
947 Canfield, D. E.: Reactive iron in marine sediments, Geochimica et cosmochimica acta, 53, 619-
948   632, 1989.
949 Canfield, D. E., Stewart, F. J., Thamdrup, B., De Brabandere, L., Dalsgaard, T., Delong, E. F.,
950   Revsbech, N. P., and Ulloa, O.: A cryptic sulfur cycle in oxygen-minimum–zone
951   waters off the Chilean coast, Science, 330, 1375-1378, 2010.
952 Charoenpong, C. N., Bristow, L. A., and Altabet, M. A.: A continuous flow isotope ratio mass
953   spectrometry method for high precision determination of dissolved gas ratios and
954   isotopic composition, Limnology and Oceanography: Methods, 12, 323-337, 2014.

Cline, J. D.: Spectrophometric determination of hydrogen sulfide in natural waters, Limnol. Oceanogr., 14, 454-458, 1969.

Dale, A. W., Bertics, V. J., Treude, T., and Wallmann, K.: Modeling benthic-pelagic nutrient exchange processes and porewater distributions in a seasonally hypoxic sediment: evidence for massive phosphate release by Beggiatoa?, Biogeosciences, 10, 629-651, 2013.

Dale, A. W., Sommer, S., Lomnitz, U., Bourbonnais, A., and Wallmann, K.: Biological nitrate transport in sediments on the Peruvian margin mitigates benthic sulfide emissions and drives pelagic N loss during stagnation events, Deep Sea Research Part I: Oceanographic Research Papers, 112, 123-136, 2016.

Dale, A. W., Sommer, S., Ryabenko, E., Noffke, A., Bohlen, L., Wallmann, K., Stolpovsky, K., Greinert, J., and Pfannkuche, O.: Benthic nitrogen fluxes and fractionation of nitrate in the Mauritanian oxygen minimum zone (Eastern Tropical North Atlantic), Geochimica et Cosmochimica Acta, 134, 234-256, 2014.

Dale, A. W., Sommer, S., Bohlen, L., Treude, T., Bertics, V. J., Bange, H. W., Pfannkuche, O., Schorp, T., Mattsdotter, M., and Wallmann, K.: Rates and regulation of nitrogen cycling in seasonally hypoxic sediments during winter (Boknis Eck, SW Baltic Sea): Sensitivity to environmental variables, Estuar. Continent. Shelf Sci., 95, 14-28, 2011.

Dale, A. W., Sommer, S., Lomnitz, U., Montes, I., Treude, T., Liebetrau, V., Gier, J., Hensen, C., Dengler, M., Stolpovsky, K., Bryant, L. D., and Wallmann, K.: Organic carbon production, mineralisation and preservation on the Peruvian margin, Biogeosciences, 12, 1537-1559, 2015.

De Brabandere, L., Bonaglia, S., Kononets, M. Y., Viktorsson, L., Stigebrandt, A., Thamdrup, B., and Hall, P. O.: Oxygenation of an anoxic fjord basin strongly stimulates benthic denitrification and DNRA, Biogeochemistry, 126, 131-152, 2015.

Emery, K., Hülsemann, J., and Rodolfo, K.: Influence of turbidity currents upon basin waters, Limnology and Oceanography, 7, 439-446, 1962.

Emmer, E. and Thunell, R. C.: Nitrogen isotope variations in Santa Barbara Basin sediments: Implications for denitrification in the eastern tropical North Pacific during the last 50,000 years, Paleoceanography, 15, 377-387, 2000.

Fossing, H., Gallardo, V. A., Jørgensen, B. B., Hüttel, M., Nielsen, L. P., Schulz, H., Canfield, D. E., Forster, S., Glud, R. N., and Gundersen, J. K.: Concentration and transport of nitrate by the mat-forming sulphur bacterium Thioploca, Nature, 374, 713-715, 1995.

García-Robledo, E., Corzo, A., and Papaspyrou, S.: A fast and direct spectrophotometric method for the sequential determination of nitrate and nitrite at low concentrations in small volumes, Marine Chemistry, 162, 30-36, 2014.

Gier, J., Sommer, S., Löscher, C. R., Dale, A. W., Schmitz, R. A., and Treude, T.: Nitrogen fixation in sediments along a depth transect through the Peruvian oxygen minimum zone, Biogeosciences, 13, 4065–4080, 2016.

Glud, R. N., Gundersen, J. K., and Ramsing, N. B.: Electrochemical and optical oxygen microsensors for in situ measurements, in: In situ monitoring of aquatic systems: Chemical analysis and speciation, edited by: Buffle, J., and Horvai, G., Wiley, 2000.

997 Goericke, R., Bograd, S. J., and Grundle, D. S.: Denitrification and flushing of the Santa Barbara
998   Basin bottom waters, Deep Sea Research Part II: Topical Studies in Oceanography, 112,
999   53-60, 2015.

1000 Grasshoff, K., Ehrhardt, M., and Kremling, K.: Methods of seawater analysis, Wiley-VCH Verlag
1001   GmbH, Weinheim1999.

1002 Gundersen, J. K. and Jørgensen, B. B.: Microstructure of diffusive boundary layers and the
1003   oxygen uptake of the sea floor, Nature, 345, 604-607, 1990.

1004 Hall, P. O. J. and Aller, R. C.: Rapid small-volume flow injection analysis for $\sum CO_2$ and NH_4^+ in
1005   marine and fresh waters, Limnol. Oceanogr., 37, 1113-1119, 1992.

1006 Hardison, A. K., Algar, C. K., Giblin, A. E., and Rich, J. J.: Influence of organic carbon and nitrate
1007   loading on partitioning between dissimilatory nitrate reduction to ammonium (DNRA)
1008   and N2 production, Geochimica et Cosmochimica Acta, 164, 146-160, 2015.

1009 Harris, D., Horwáth, W. R., and Van Kessel, C.: Acid fumigation of soils to remove carbonates
1010   prior to total organic carbon or carbon‐13 isotopic analysis, Soil Science Society of
1011   America Journal, 65, 1853-1856, 2001.

1012 Hermans, M., Lenstra, W. K., Hidalgo-Martinez, S., van Helmond, N. A., Witbaard, R.,
1013   Meysman, F. J., Gonzalez, S., and Slomp, C. P.: Abundance and biogeochemical impact
1014   of cable bacteria in Baltic Sea sediments, Environmental science & technology, 53,
1015   7494-7503, 2019.

1016 Hossain, M., Bhattacharya, P., Frape, S. K., Jacks, G., Islam, M. M., Rahman, M. M., von
1017   Brömssen, M., Hasan, M. A., and Ahmed, K. M.: Sediment color tool for targeting
1018   arsenic-safe aquifers for the installation of shallow drinking water tubewells, Science
1019   of the Total Environment, 493, 615-625, 2014.

1020 Huettel, M., Forster, S., Kloser, S., and Fossing, H.: Vertical migration in the sediment-dwelling
1021   sulfur bacteria Thioploca spp. in overcoming diffusion limitations, Applied and
1022   Environmental Microbiology, 62, 1863-1872, 1996.

1023 Hylén, A., Bonaglia, S., Robertson, E., Marzocchi, U., Kononets, M., and Hall, P. O.: Enhanced
1024   benthic nitrous oxide and ammonium production after natural oxygenation of long‐
1025   term anoxic sediments, Limnology and Oceanography, 67, 419-433, 2022.

1026 Høgslund, S., Revsbech, N. P., Kuenen, J. G., Jørgensen, B. B., Gallardo, V. A., Vossenberg, J. v.
1027   d., Nielsen, J. L., Holmkvist, L., Arning, E. T., and Nielsen, L. P.: Physiology and
1028   behaviour of marine Thioploca, The ISME journal, 3, 647-657, 2009.

1029 Jeroschewsky, P., Steuckart, C., and Kuehl, M.: An amperometric microsensor for the
1030   determination af H2S in aquatic environments, Anal. Chem., 68, 4351-4357, 1996.

1031 Jørgensen, B.: Distribution of colorless sulfur bacteria (Beggiatoa spp.) in a coastal marine
1032   sediment, Marine Biology, 41, 19-28, 1977.

1033 Jørgensen, B. B.: A comparison of methods for the quantification of bacterial sulphate
1034   reduction in coastal marine sediments: I. Measurements with radiotracer techniques,
1035   Geomicrobiol. J., 1, 11-27, 1978.

1036 Jørgensen, B. B. and Nelson, D. C.: Sulfide oxidation in marine sediments: Geochemistry meets
1037   microbiology, Geological Society of America, Special Paper 379, 63-81, 2004.

1038 Kallmeyer, J., Ferdelman, T. G., Weber, A., Fossing, H., and Jørgensen, B. B.: A cold chromium
1039   distillation procedure for radiolabeled sulfide applied to sulfate reduction
1040   measurements, Limnol. Oceanogr. Methods, 2, 171-180, 2004.
1041 Kamp, A., Høgslund, S., Risgaard-Petersen, N., and Stief, P.: Nitrate storage and dissimilatory
1042   nitrate reduction by eukaryotic microbes, Frontiers in microbiology, 6, 1492, 2015.
1043 Kamp, A., de Beer, D., Nitsch, J. L., Lavik, G., and Stief, P.: Diatoms respire nitrate to survive
1044   dark and anoxic conditions, Proceedings of the National Academy of Sciences, 108,
1045   5649-5654, 2011.
1046 Kessler, A. J., Wawryk, M., Marzocchi, U., Roberts, K. L., Wong, W. W., Risgaard–Petersen, N.,
1047   Meysman, F. J., Glud, R. N., and Cook, P. L.: Cable bacteria promote DNRA through iron
1048   sulfide dissolution, Limnology and Oceanography, 64, 1228-1238, 2019.
1049 Kjeldsen, K. U., Schreiber, L., Thorup, C. A., Boesen, T., Bjerg, J. T., Yang, T., Dueholm, M. S.,
1050   Larsen, S., Risgaard-Petersen, N., and Nierychlo, M.: On the evolution and physiology
1051   of cable bacteria, Proceedings of the National Academy of Sciences, 116, 19116-19125,
1052   2019.
1053 Kononets, M., Tengberg, A., Nilsson, M., Ekeroth, N., Hylén, A., Robertson, E. K., Van De Velde,
1054   S., Bonaglia, S., Rütting, T., and Blomqvist, S.: In situ incubations with the Gothenburg
1055   benthic chamber landers: Applications and quality control, Journal of Marine Systems,
1056   214, 103475, 2021.
1057 Kraft, B., Tegetmeyer, H. E., Sharma, R., Klotz, M. G., Ferdelman, T. G., Hettich, R. L., Geelhoed,
1058   J. S., and Strous, M.: The environmental controls that govern the end product of
1059   bacterial nitrate respiration, Science, 345, 676-679, 2014.
1060 Kuwabara, J. S., van Geen, A., McCorkle, D. C., and Bernhard, J. M.: Dissolved sulfide
1061   distributions in the water column and sediment pore waters of the Santa Barbara
1062   Basin, Geochimica et Cosmochimica Acta, 63, 2199-2209, 1999.
1063 Lazo-Murphy, B. M., Larson, S., Staines, S., Bruck, H., McHenry, J., Bourbonnais, A., and Peng,
1064   X.: Nitrous oxide production and isotopomer composition by fungi isolated from salt
1065   marsh sediments, Frontiers in Marine Science, 9, 1098508, 2022.
1066 Levin, L. A., Gutierrez, D., Rathburn, A. E., Neira, C., Sellanes, J., Munoz, P., Gallardo, V. A., and
1067   Salamance, M.: Bethic processes on the Peru margin: a transect across the oxygen
1068   minimum zone during the 1997-98 El Nino, Prog. Oceanog., 53, 1-27, 2002.
1069 Marchant, H. K., Lavik, G., Holtappels, M., and Kuypers, M. M.: The fate of nitrate in intertidal
1070   permeable sediments, PloS one, 9, e104517, 2014.
1071 Marzocchi, U., Bonaglia, S., van de Velde, S., Hall, P. O., Schramm, A., Risgaard–Petersen, N.,
1072   and Meysman, F. J.: Transient bottom water oxygenation creates a niche for cable
1073   bacteria in long–term anoxic sediments of the Eastern Gotland Basin, Environmental
1074   microbiology, 20, 3031-3041, 2018.
1075 Marzocchi, U., Trojan, D., Larsen, S., Louise Meyer, R., Peter Revsbech, N., Schramm, A., Peter
1076   Nielsen, L., and Risgaard-Petersen, N.: Electric coupling between distant nitrate
1077   reduction and sulfide oxidation in marine sediment, The ISME journal, 8, 1682-1690,
1078   2014.
1079 Middelburg, J. and Levin, L.: Coastal hypoxia and sediment biogeochemistry, Biogeosciences,
1080   6, 1273-1293, 2009.

1081   Mortimer, C. H.: The exchange of dissolved substances between mud and water in lakes,
1082   Journal of ecology, 29, 280-329, 1941.
1083   Mosch, T., Sommer, S., Dengler, M., Noffke, A., Bohlen, L., Pfannkuche, O., Liebetrau, V., and
1084   Wallmann, K.: Factors influencing the distribution of epibenthic megafauna across the
1085   Peruvian oxygen minimum zone, Deep Sea Research Part I: Oceanographic Research
1086   Papers, 68, 123-135, 2012.
1087   Mußmann, M., Schulz, H. N., Strotmann, B., Kjær, T., Nielsen, L. P., Rosselló-Mora, R. A.,
1088   Amann, R. I., and Jørgensen, B. B.: Phylogeny and distribution of nitrate-storing
1089   Beggiatoa spp. in coastal marine sediments, Environmental Microbiology, 5, 523-533,
1090   2003.
1091   Myhre, S. E., Pak, D., Borreggine, M., Kennett, J. P., Nicholson, C., Hill, T. M., and Deutsch, C.:
1092   Oxygen minimum zone biotic baseline transects for paleoceanographic reconstructions
1093   in Santa Barbara Basin, CA, Deep Sea Research Part II: Topical Studies in
1094   Oceanography, 150, 118-131, 2018.
1095   Naik, R., Naqvi, S., and Araujo, J.: Anaerobic carbon mineralisation through sulphate reduction
1096   in the inner shelf sediments of eastern Arabian Sea, Estuaries and Coasts, 40, 134-144,
1097   2017.
1098   Noffke, A., Sommer, S., Dale, A., Hall, P., and Pfannkuche, O.: Benthic nutrient fluxes in the
1099   Eastern Gotland Basin (Baltic Sea) with particular focus on microbial mat ecosystems,
1100   Journal of Marine Systems, 158, 1-12, 2016.
1101   Noffke, A., Hensen, C., Sommer, S., Scholz, F., Bohlen, L., Mosch, T., Graco, M., and Wallmann,
1102   K.: Benthic iron and phosphorus fluxes across the Peruvian oxygen minimum zone,
1103   Limnol. Oceanogr., 57, 851-867, 2012.
1104   Pavlova, G. Y., Tishchenko, P. Y., Volkova, T., Dickson, A., and Wallmann, K.: Intercalibration of
1105   Bruevich's method to determine the total alkalinity in seawater, Oceanology, 48, 438-
1106   443, 2008.
1107   Peng, X., Ji, Q., Angell, J. H., Kearns, P. J., Yang, H. J., Bowen, J. L., and Ward, B. B.: Long-term
1108   fertilization alters the relative importance of nitrate reduction pathways in salt marsh
1109   sediments, Journal of Geophysical Research: Biogeosciences, 121, 2082-2095, 2016.
1110   Peng, X., Yousavich, D. J., Bourbonnais, A., Wenzhoefer, F., Janssen, F., Treude, T., and
1111   Valentine, D. L.: The fate of fixed nitrogen in Santa Barbara Basin sediments during
1112   seasonal anoxia, EGUsphere, 2023, 1-26, 2023.
1113   Pfeffer, C., Larsen, S., Song, J., Dong, M., Besenbacher, F., Meyer, R. L., Kjeldsen, K. U.,
1114   Schreiber, L., Gorby, Y. A., and El-Naggar, M. Y.: Filamentous bacteria transport
1115   electrons over centimetre distances, Nature, 491, 218-221, 2012.
1116   Plass, A., Schlosser, C., Sommer, S., Dale, A. W., Achterberg, E. P., and Scholz, F.: The control of
1117   hydrogen sulfide on benthic iron and cadmium fluxes in the oxygen minimum zone off
1118   Peru, Biogeosciences, 17, 3685-3704, 2020.
1119   Porubsky, W., Weston, N., and Joye, S.: Benthic metabolism and the fate of dissolved
1120   inorganic nitrogen in intertidal sediments, Estuarine, Coastal and Shelf Science, 83,
1121   392-402, 2009.

1122 Preisler, A., De Beer, D., Lichtschlag, A., Lavik, G., Boetius, A., and Jørgensen, B. B.: Biological
1123   and chemical sulfide oxidation in a Beggiatoa inhabited marine sediment, ISME
1124   Journal, 341-351, 2007.
1125 Prokopenko, M., Hammond, D., Berelson, W., Bernhard, J., Stott, L., and Douglas, R.: Nitrogen
1126   cycling in the sediments of Santa Barbara basin and Eastern Subtropical North Pacific:
1127   Nitrogen isotopes, diagenesis and possible chemosymbiosis between two lithotrophs
1128   (Thioploca and Anammox)—"riding on a glider", Earth and Planetary Science Letters,
1129   242, 186-204, 2006.
1130 Qin, Q., Kinnaman, F. S., Gosselin, K. M., Liu, N., Treude, T., and Valentine, D. L.: Seasonality of
1131   Water Column Methane Oxidation and Deoxygenation in a Dynamic Marine
1132   Environment, Geochimica et Cosmochimica Acta, 2022.
1133 Raiswell, R. and Canfield, D. E.: The iron biogeochemical cycle past and present, Geochemical
1134   perspectives, 1, 1-2, 2012.
1135 Reimers, C. E., Ruttenberg, K. C., Canfield, D. E., Christiansen, M. B., and Martin, J. B.:
1136   Porewater pH and authigenic phases formed in the uppermost sediments of Santa
1137   Barbara Basin, Geochim. Cosmochim. Acta, 60, 4037-4057, 1996.
1138 Revsbech, N. P. and Jørgensen, B. B.: Microelectrodes: their use in microbial ecology, in: Adv.
1139   Microb. Ecol., edited by: Marshall, K. C., Plenum, New York, 293-352, 1986.
1140 Risgaard-Petersen, N., Langezaal, A. M., Ingvardsen, S., Schmid, M. C., Jetten, M. S. M., Op den
1141   Camp, H. J. M., Derksen, J. W. M., Pina-Ochoa, E., Eriksson, S. P., Nielsen, L. P.,
1142   Revsbech, N. P., Cedhagen, T., and Zwaan van der, G. J.: Evidence for complete
1143   denitrification in a benthic foraminifer, Nature, 443, 93-96, 2006.
1144 Robinson, D. M., Pham, A. L., Yousavich, D. J., Janssen, F., Wenzhöfer, F., Arrington, E. C.,
1145   Gosselin, K. M., Sandoval-Belmar, M., Mar, M., and Valentine, D. L.: Iron "Ore"
1146   Nothing: Benthic iron fluxes from the oxygen-deficient Santa Barbara Basin enhance
1147   phytoplankton productivity in surface waters, Biogeosciences Discussions, 1-36, 2022.
1148 Sayama, M.: Presence of nitrate-accumulating sulfur bacteria and their influence on nitrogen
1149   cycling in a shallow coastal marine sediment, Applied and Environmental Microbiology,
1150   67, 3481-3487, 2001.
1151 Schauer, R., Risgaard-Petersen, N., Kjeldsen, K. U., Tataru Bjerg, J. J., B Jørgensen, B.,
1152   Schramm, A., and Nielsen, L. P.: Succession of cable bacteria and electric currents in
1153   marine sediment, The ISME journal, 8, 1314-1322, 2014.
1154 Schroller-Lomnitz, U., Hensen, C., Dale, A. W., Scholz, F., Clemens, D., Sommer, S., Noffke, A.,
1155   and Wallmann, K.: Dissolved benthic phosphate, iron and carbon fluxes in the
1156   Mauritanian upwelling system and implications for ongoing deoxygenation, Deep Sea
1157   Research Part I: Oceanographic Research Papers, 143, 70-84, 2019.
1158 Schulz, H. N. and Schulz, H. D.: Large sulfur bacteria and the formation of phosphorite,
1159   Science, 307, 416-418, 2005.
1160 Schulz, H. N., Jorgensen, B. B., Fossing, H. A., and Ramsing, N. B.: Community structure of
1161   filamentous, sheath-building sulfur bacteria, Thioploca spp., off the coast of Chile,
1162   Applied and Environmental Microbiology, 62, 1855-1862, 1996.
1163 Schulz, H. N., Brinkhoff, T., Ferdelman, T. G., Hernández Mariné, M., Teske, A., and Jørgensen,
1164   B. B.: Dense populations of a giant sulfur bacterium in Namibian shelf sediments,
1165   Science, 284, 493-495, 1999.

1166   Seitaj, D., Schauer, R., Sulu-Gambari, F., Hidalgo-Martinez, S., Malkin, S. Y., Burdorf, L. D.,
1167   Slomp, C. P., and Meysman, F. J.: Cable bacteria generate a firewall against euxinia in
1168   seasonally hypoxic basins, Proceedings of the National Academy of Sciences, 112,
1169   13278-13283, 2015.
1170   Sholkovitz, E.: Interstitial water chemistry of the Santa Barbara Basin sediments, Geochimica
1171   et Cosmochimica Acta, 37, 2043-2073, 1973.
1172   Sholkovitz, E. R. and Gieskes, J. M.: A PHYSICAL–CHEMICAL STUDY OF THE FLUSHING OF THE
1173   SANTA BARBARA BASIN 1, Limnology and Oceanography, 16, 479-489, 1971.
1174   Sigman, D. M., Robinson, R., Knapp, A., Van Geen, A., McCorkle, D., Brandes, J., and Thunell,
1175   R.: Distinguishing between water column and sedimentary denitrification in the Santa
1176   Barbara Basin using the stable isotopes of nitrate, Geochemistry, Geophysics,
1177   Geosystems, 4, 2003.
1178   Sommer, S., Gier, J., Treude, T., Lomnitz, U., Dengler, M., Cardich, J., and Dale, A. W.:
1179   Depletion of oxygen, nitrate and nitrite in the Peruvian oxygen minimum zone cause
1180   an imbalance of benthic nitrogen fluxes, Deep-Sea Res. I, 112, 113–122, 2016.
1181   Stramma, L., Johnson, G. C., Sprintall, J., and Mohrholz, V.: Expanding oxygen-minimum zones
1182   in the tropical oceans, Science, 320, 655-658, 2008.
1183   Sverdrup, H. and Allen, W.: Distribution of diatoms in relation to the character of water
1184   masses and currents off Southern California in 1938, J. mar. Res, 2, 131-144, 1939.
1185   Thunell, R. C.: Particle fluxes in a coastal upwelling zone: sediment trap results from Santa
1186   Barbara Basin, California, Deep Sea Research Part II: Topical Studies in Oceanography,
1187   45, 1863-1884, 1998.
1188   Tiedje, J. M., Sexstone, A. J., Myrold, D. D., and Robinson, J. A.: Denitrification: ecological
1189   niches, competition and survival, Antonie van Leeuwenhoek, 48, 569-583, 1983.
1190   Treude, T.: Biogeochemical reactions in marine sediments underlying anoxic water bodies, in:
1191   Anoxia: Paleontological Strategies and Evidence for Eukaryote Survival, edited by:
1192   Altenbach, A., Bernhard, J., and Seckbach, J., Cellular Origins, Life in Extreme Habitats
1193   and Astrobiology (COLE) Book Series, Springer, Dordrecht, 18-38, 2011.
1194   Treude, T., Hamdan, L. J., Lemieux, S., Dale, A. W., and Sommer, S.: Rapid sulfur cycling in
1195   sediments from the Peruvian oxygen minimum zone featuring simultaneous sulfate
1196   reduction and sulfide oxidation, Limnology and Oceanography, 66, 2661-2671, 2021.
1197   Treude, T., Smith, C. R., Wenzhoefer, F., Carney, E., Bernardino, A. F., Hannides, A. K., Krueger,
1198   M., and Boetius, A.: Biogeochemistry of a deep-sea whale fall: sulfate reduction,
1199   sulfide efflux and methanogenesis, Mar. Ecol. Prog. Ser., 382, 1-21, 2009.
1200   Valentine, D. L., Fisher, G. B., Pizarro, O., Kaiser, C. L., Yoerger, D., Breier, J. A., and Tarn, J.:
1201   Autonomous marine robotic technology reveals an expansive benthic bacterial
1202   community relevant to regional nitrogen biogeochemistry, Environmental science &
1203   technology, 50, 11057-11065, 2016.
1204   Van Cappellen, P. and Ingall, E. D.: Benthic phosphorus regeneration, net primary production,
1205   and ocean anoxia: A model of the coupled marine biogeochemical cycles of carbon and
1206   phosphorus, Paleoceanography, 9, 677-692, 1994.
1207   Van De Velde, S., Lesven, L., Burdorf, L. D., Hidalgo-Martinez, S., Geelhoed, J. S., Van Rijswijk,
1208   P., Gao, Y., and Meysman, F. J.: The impact of electrogenic sulfur oxidation on the

1209   biogeochemistry of coastal sediments: A field study, Geochimica et Cosmochimica

1210   Acta, 194, 211-232, 2016.

1211 van de Velde, S. J., Hylén, A., Eriksson, M., James, R. K., Kononets, M. Y., Robertson, E. K., and

1212   Hall, P. O.: Exceptionally high respiration rates in the reactive surface layer of

1213   sediments underlying oxygen-deficient bottom waters, Proceedings of the Royal

1214   Society A, 479, 20230189, 2023.

1215 van de Velde, S. J., Hylén, A., Kononets, M., Marzocchi, U., Leermakers, M., Choumiline, K.,

1216   Hall, P. O., and Meysman, F. J.: Elevated sedimentary removal of Fe, Mn, and trace

1217   elements following a transient oxygenation event in the Eastern Gotland Basin, central

1218   Baltic Sea, Geochimica et Cosmochimica Acta, 271, 16-32, 2020.

1219 Wallmann, K., José, Y. S., Hopwood, M. J., Somes, C. J., Dale, A. W., Scholz, F., Achterberg, E.

1220   P., and Oschlies, A.: Biogeochemical feedbacks may amplify ongoing and future ocean

1221   deoxygenation: a case study from the Peruvian oxygen minimum zone,

1222   Biogeochemistry, 159, 45-67, 2022.

1223 Ward, B., Devol, A., Rich, J., Chang, B., Bulow, S., Naik, H., Pratihary, A., and Jayakumar, A.:

1224   Denitrification as the dominant nitrogen loss process in the Arabian Sea, Nature, 461,

1225   78-81, 2009.

1226 Zhang, L., Altabet, M. A., Wu, T., and Hadas, O.: Sensitive measurement of NH4+ 15N/14N

1227   (δ15NH4+) at natural abundance levels in fresh and saltwaters, Analytical Chemistry,

1228   79, 5297-5303, 2007.

1229 Zopfi, J., Kjær, T., Nielsen, L. P., and Jørgensen, B. B.: Ecology of Thioploca spp.: nitrate and

1230   sulfur storage in relation to chemical microgradients and influence of Thioploca spp.

1231   on the sedimentary nitrogen cycle, Applied and Environmental Microbiology, 67, 5530-

1232   5537, 2001.

1233

1234